LitAR: Visually Coherent Lighting for Mobile Augmented Reality

ANONYMOUS AUTHOR(S)
SUBMISSION ID: 2991

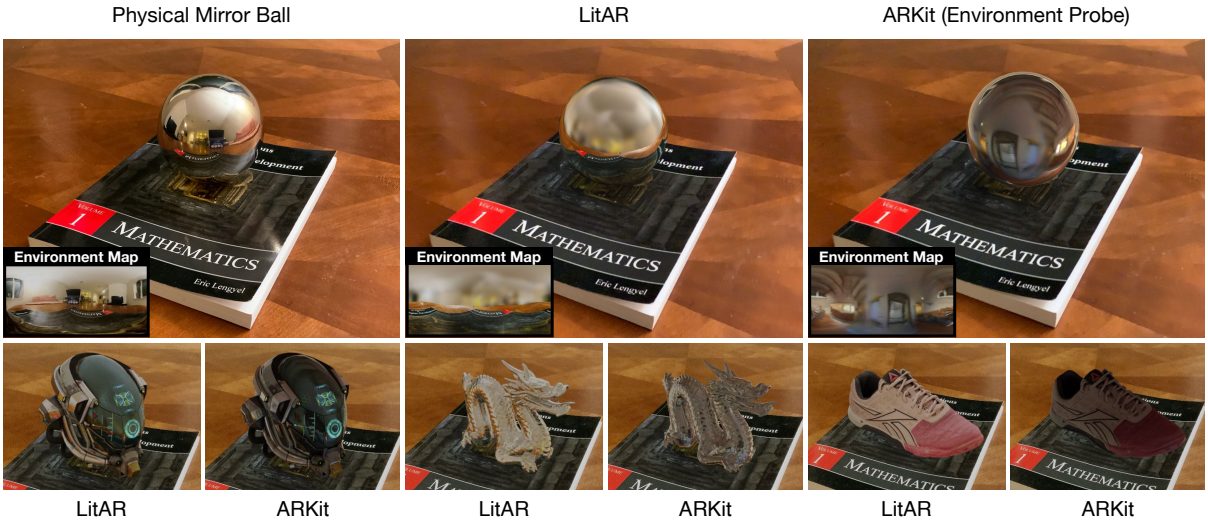

Fig. 1. ***Rendered objects with LitAR compared to physical mirror ball and with ARKit [34].*** *Row 1:* LitAR produces visually-coherent reflective rendering while ARKit doesn't; the bottom part of ARKit-rendered ball does not faithfully reflect the book cover. The top part of LitAR-rendered ball has an intentionally gradient blurring effect for quality-time trade-offs (see §4.2). *Row 2:* LitAR achieves more realistic and visually coherent rendering effects than ARKit for objects with different materials.

An accurate understanding of omnidirectional environment lighting is crucial for high-quality virtual object rendering in mobile augmented reality (AR). In particular, to support reflective rendering, existing methods have leveraged deep learning models to estimate or physical light probes to capture physical lighting, often in the form of an environment map. However, these methods often fail to provide visually coherent details or require additional setup. For example, the commercial framework ARKit uses a convolutional neural network to generate realistic environment maps which might not match the physical environments, as we observed. In this work, we design and implement a lighting reconstruction framework called LitAR that enables realistic and visually-coherent rendering. LitAR addresses several challenges of supporting lighting information for mobile AR.

First, to address the spatial variance problem, LitAR divides the lighting reconstruction task into the spatial variance-aware near-field reconstruction and the directional-aware far-field reconstruction, called two-field lighting reconstruction.

2474-9567/2022/8-ART111 $15.00
https://doi.org/XXXXXXX.XXXXXXX

The corresponding environment map allows reflective rendering with correct color tones. Second, LitAR has two noise-tolerant data capturing policies called guided bootstrapped movement and motion-based automatic capturing to ensure data quality. Third, to handle the mismatch between the mobile computation and the high computation requirement of lighting reconstruction, LitAR employs two novel real-time environment map rendering techniques called multi-resolution projection and anchor extrapolation. These two techniques effectively free LitAR from needing time-consuming mesh reconstruction without sacrificing visual quality. Lastly, LitAR provides several knobs to facilitate mobile AR application developers to make lighting reconstruction quality and performance trade-offs. We evaluate the performance of LitAR using a small-scale testbed experiment and a controlled simulation. Our testbed-based evaluation shows that LitAR achieves more visually coherent rendering effects than ARKit. Our design of multi-resolution projection significantly reduces the point cloud projection time from about 3 seconds to 14.6ms. Our simulation shows that LitAR, on average, achieves up to 44.1% higher PSNR value than a recent work Xihe on two complex objects with physically-based materials.

CCS Concepts: • **Computing methodologies** → **Mixed / augmented reality**; • **Human-centered computing** → **Ubiquitous and mobile computing systems and tools**; • **Computer systems organization** → **Distributed architectures**.

Additional Key Words and Phrases: mobile augmented reality; lighting estimation; 3D vision

ACM Reference Format:
Anonymous Author(s). 2022. LitAR: Visually Coherent Lighting for Mobile Augmented Reality. *Proc. ACM Interact. Mob. Wearable Ubiquitous Technol.* 37, 4, Article 111 (August 2022), 27 pages. https://doi.org/XXXXXXX.XXXXXXX

1 INTRODUCTION

Mobile augmented reality (AR) has attracted increasing interest from both academia and industry as a means to better engage users by allowing seamless integration of physical and virtual environments [3, 27, 35]. The current mobile AR ecosystem is infused with new hardware development [32], improved frameworks [34], advancing vision and graphics algorithms [65], and end-user facing applications ranging from e-commerce ones to educational ones [2].

Given the interactive nature of AR applications, users often prefer virtual objects of high visual quality. That is, the rendered virtual objects should look realistic and feel like they belong to the physical surroundings, a property commonly referred to as *visual coherence*. For example, virtual sunglasses that are overlayed on a user's face should look like physical sunglasses (realistic) and reflect the correct physical environment (visual coherence). In order to achieve both realistic and visually coherent rendering, mobile AR applications require access to an accurate representation of omnidirectional environment lighting (often represented as *environment map* for image-based lighting) at the user-specified rendering position [47, 65].

However, obtaining a high-quality environment map for mobile AR has to overcome several key challenges. First, the inherently spatial variation of indoor environment lighting makes the environment map at the *observation position*—which can be more easily reconstructed with more camera observations—an ill approximation of *rendering position* environment map. This challenge was demonstrated in prior work [24, 65] and our motivating example. Second, the natural user mobility associated with mobile AR usage can induce noise to necessary data (such as 6DoF tracking and RGB image data) for lighting estimation. For example, we observe that the tracking data provided by ARKit can show that consecutive camera frames are misaligned, although they represent the same physical space. Third, mobile devices can have heterogeneous sensing capability, e.g., in cameras' Field-of-view (FoV) range or their depth-sensing ability, which makes it necessary to consider auxiliary components (such as depth estimation [1, 48, 64]) for obtaining accurate lighting. Fourth, mobile devices have relatively limited resources compared to their desktop counterpart, while the interactivity nature often requires 30FPS rendering. The computational limitation makes it challenging to directly use computational-intensive models designed to run on powerful GPU servers [53], and motivates sparse usage or optimization of time-consuming operations (such as point cloud registration [9] and mesh reconstruction [8]) as possible.

In this work, we investigate the problem of *providing high-quality lighting information for mobile AR* by addressing the above four key challenges. Our key goal is to support both realistic and visually coherent rendering of virtual objects with various geometries and materials. Figure 1 compares the visual effect of virtual objects rendered with lighting information obtained with our proposed system called LitAR and ARKit. We show that LitAR achieves high-quality rendering with structurally similar reflections with the physical object and more visually coherent reflection than objects rendered with ARKit.

LitAR involves a novel technique called *two-field lighting reconstruction* and several complementary components that work together to deliver a high-quality environment map with low-performance impact. Specifically, we design two-field lighting reconstruction with the insight of dividing the camera observations into two types, the near-field, and far-field observations, to speed up lighting reconstruction while maintaining the visual quality. This technique shares a similar spirit to the well-known screen space reflection [42] and is tailored to mobile AR by fully exploring user mobility. Specifically, LitAR generates a multi-view dense point cloud to represent the *near field*, the portion of the environment map that receives more accurate and higher confidence depth information surrounding the rendering position. This design helps produce geometrically accurate lighting transformation between the observation and rendering positions, thus supporting key rendering features like reflections and providing visual coherence. Further, LitAR leverages far-field observations to handle the anisotropic property of lighting by reconstructing sparse point clouds to reduce visual errors.

On top of the two-field lighting reconstruction, we incorporate two noise-tolerant data capturing policies—guided bootstrapped movement and motion-based automatic capturing—to improve the data quality. The *guided bootstrapped movement* policy directs the camera views to more efficiently capture required near-field and far-field observations. This policy also brings other benefits, such as enlarged FoVs and reduced user movement and time needed for reconstructing high-quality lighting. It is worth noting that LitAR can leverage new observations, e.g., device orientation and user movement, to progressively improve the quality of the environment map. The *motion-based automatic capturing* policy leverages multi-sensory information to capture spatially and temporally new observations. Moreover, we propose two performance optimizations that significantly reduce the time reconstructing the final environment map from the intermediate 3D point clouds. The first optimization uses a lightweight multi-resolution projection instead of the traditional expensive mesh reconstruction to generate the near-field portion. The second optimization uses a unit sphere-based approach called *anchor extrapolation* to generate gradient coloring and blurring effect of the far-field portion. Lastly, LitAR supports reconstruction quality and time trade-offs to account for dynamic lighting conditions. By default, LitAR provides three quality presets for mobile AR developers.

We implement LitAR as an edge-assisted framework that consists of about 2.2K lines of code running on both the mobile device and the edge server. Specifically, the client-side component works with various sensors, including camera, depth, and motion sensors, to capture both near-field and far-field observations. The resulting data is encoded and sent to the edge server to generate multi-view dense point clouds with good alignment and visual pixel continuity, and a fixed-size unit sphere point cloud. Mobile AR applications built with Unity ARFoundation can directly use LitAR to render realistic virtual objects; we also implement a reference iOS AR application for our testbed-based evaluation. To evaluate LitAR in a controlled environment, we also develop an Unreal Engine-based simulator that exposes multiple knobs for controlling physical factors such as camera location and FoV, and provides ground truth lighting information. The testbed-based system evaluation shows that LitAR achieves more visually coherent rendering effects than ARKit and higher PSNR/SSIM values for three real-world scenes. The end-to-end latency measurements show that LitAR can generate about 22 environment maps per second, effectively supporting 22 fps which is sufficient for most mobile AR applications [62, 63]. Our simulator-based evaluations involve one realistic indoor scene and six virtual objects of different shapes and materials. We evaluate LitAR's performance with various observation-rendering position pairs. We show that

it achieves 36.7% and 17.1% higher rendering PSNR when compared to a recent deep learning-based lighting approach [66] and environment lighting captured by 360° cameras at the observation position, respectively.

Related work on generating spatial-variant lighting includes classical physical probe-based techniques [15, 16, 47] and learning-based solutions [24, 52, 53, 65]. Physical probe-based techniques can often produce high-quality environment maps but have more constrained usage scenarios since they require additional setup [52]. On the other hand, the applicability of learning-based solutions is often limited by the access to large training datasets, e.g., Matterport3D [11], and their suitability to run on heterogeneous mobile devices [53]. Another side effect is the difficulty of conducting comprehensive comparisons due to the lack of publicly available source code and benchmark dataset [52]. In this work, we are interested in designing a mobile-specific lighting framework that circumvents the limitations mentioned above by considering mobile characteristics from the outset. Compared to a recent work by Somanath et al. [52] that generates HDR environment maps using a neural network trained leveraging adversarial training, LitAR has the advantage of simplicity yet achieving good visual coherence.

In summary, we make the following key contributions:

- We design a novel technique called two-field lighting reconstruction which can be used to generate high-quality environment maps from mobile cameras with limited FoV. Each environment map consists of near-field and far-field portions that are separately constructed from near-field and far-field observations. The resulting environment map captures both spatial and directional variances and is suitable for reflective rendering.
- We develop a number of complementary techniques to handle mobility-induced noise, limited mobile sensing capabilities, and the computation intensity that naturally arises during the lighting reconstruction process. For example, our multi-resolution projection and anchor extrapolation techniques efficiently project the intermediate 3D point clouds to the final 2D environment maps. These techniques ensure high data input quality, good usability, and low reconstruction time.
- We implement all the techniques in an edge-assisted system called LitAR and develop an Unreal Engine-based simulator. The system implementation provides a platform to compare LitAR to the commercial framework ARKit. The simulator facilitates controlled experiments and allows easy comparisons between lighting techniques and ground truth lighting. Our source code and related artifacts will be released to encourage follow-up research.
- We evaluate the performance of LitAR on a small-scale testbed using the simulator. The testbed-based system evaluation shows that LitAR (at all three quality presets) outperforms ARKit in three real-world indoor scenes. LitAR also delivers environment maps at 22fps and higher depending on the quality settings. The simulation-based evaluation shows that LitAR can achieve up to 36.7% better PSNR value on objects with various geometries and materials than a recent lighting framework [66].

2 BACKGROUND: LIGHTING FOR MOBILE AR

Obtaining lighting information is a classic problem in computer vision and graphics [20]. Having access to accurate environment lighting information is crucial to many application domains such as 3D object composition [23] and portrait relighting [46] and can lead to photorealistic rendering.

As mobile device capability increases and AR re-emerges in user-facing applications [2, 35], obtaining environment lighting for photorealistic rendering has garnered increased interests in various research communities [12, 47, 52, 65, 66]. In addition to these mobile-specific lighting works, researchers have investigated image-based lighting [14, 15, 36], generating environment lighting representations from camera videos [28, 30, 59], and assisted lighting reconstruction with physical probes [16], object cues [55], or scene geometry [6, 41]. Recent work is mostly deep learning-based and can be broadly categorized based on the output: estimating low-frequency lighting [24, 66] or high-quality lighting [22, 53].

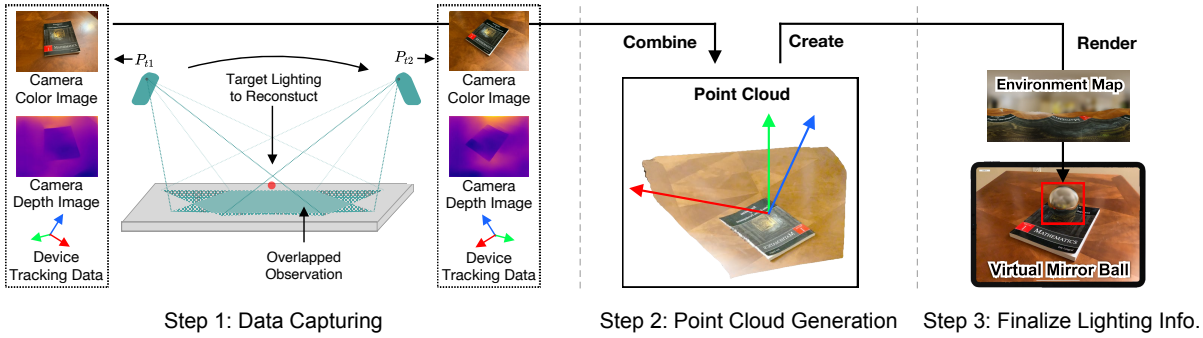

Fig. 2. ***A simplified workflow of mobile AR lighting reconstruction.*** In this example, the mobile device starts at position P_{t1} and points toward the mobile user-specified rendering position at the table. Data such as color and depth image, as well as device tracking data will be captured. The device will further captures more data (e.g., color/depth images from a different viewing direction) at position P_{t2}, which naturally overlaps with the data captured at P_{t1}. The data will be maintained in a fixed size buffer and combined to generate a global multi-view point cloud. The point cloud will be updated as new data arrives and be used to generate the final environment map for virtual object rendering.

In this paper, we aim to provide lighting support for mobile augmented reality (AR), an emerging application that augments the real world by overlaying with virtual objects in indoor scenes. Our work will develop a non-learning-based approach by leveraging *lighting reconstruction* (§2.1), to address the following two issues: *(i)* the typical limitations of DL-based methods like training data availability and inference performance on heterogeneous mobile resources; *(ii)* the underexploited mobile characteristics. Note that techniques commonly used for creating realistic virtual worlds, such are screen space rendering [42] that only ray traces what is being presented on the screen, can fall short in delivering the visual coherence required by AR. This shortcoming is mainly due to the key difference in perceivable lighting impact on virtual objects; unlike in fully virtualized environments, AR users can observe environment lighting outside screen space and potentially perceive incoherent visual effects.

Further, we will focus on developing lighting understanding techniques assuming image-based rendering [15], e.g., generating lighting representation in the form of an environment map to render virtual objects with different materials. Our key goal is to generate high-quality environment maps for visually coherent rendering for mobile AR while keeping the time cost low. Specifically, we aim to reduce the overall time to obtain the final environment map and reduce the component-wise time for intermediate outputs (such as point cloud projection).

2.1 Lighting Reconstruction Premier

In this section, we present the critical information of *multi-view lighting reconstruction* (refer to Figure 2), which serves as the basis for understanding our proposed lighting reconstruction framework LitAR. At a high level, we define *lighting reconstruction* as a similar task to the multi-view 3D reconstruction [10, 43] with the key difference in the reconstruction target. Our key insight is that by leveraging multiple captures of the physical environment that are often required by commercial AR frameworks [25, 34], we can use similar techniques used by 3D reconstruction to build understanding regarding environment lighting. Conceptually simple, we have to address several challenges specific to the mobile AR environment (detailed in §3). Next, we describe the general procedure for the lighting reconstruction task.

- *Step 1: Capturing Environment Data.* There are a number of different types of data, e.g., color images and depth information, that are needed in lighting reconstruction, The common way to obtain these required data is

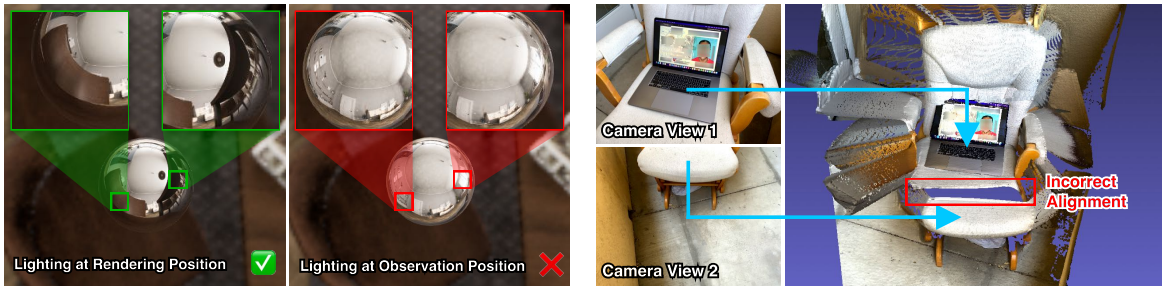

(a) Lighting variance **(b)** Mobility-induced noise

Fig. 3. ***Motivating examples.*** (a) illustrates the spatial lighting variance of a same mirror ball object rendered with environment map at AR mobile device's position and mirror ball placement position. (b) shows the mobility induced tracking noise on misaligned point cloud generated from two consecutive frames.

to directly leverage a modern mobile device with a reasonable camera and have the mobile AR users move the mobile device to scan the surroundings manually. The resulting captured data are often in the LDR or HDR image formats, which can then be used to reconstruct the environment's appearance and geometry. To improve the reconstruction quality and performance, one can also resort to additional setups such as the use of a physical chrome ball [15, 47] or additional mobile sensors such as depth sensors [31, 32] or accelerometers. Ambient light sensors can also be used to observe the environment's ambient color, which can be used to match the object's color tone with the environment's lighting. This work focuses on mobile devices that can capture color and depth images and provide device tracking data, e.g., a LiDAR-enabled iPad Pro. Data will be captured from different viewing positions and used in the next step for generating a multi-view point cloud.

- *Step 2: Generating Point Cloud.* Similar to other 3D reconstruction tasks [10, 43], we can convert the camera color and depth images and device tracking data into a point cloud representation in the same world space. Using the point cloud data structure allows us to combine the subsequent view data more efficiently than directly stitching 2D images. Two practical issues often need to be addressed. First, real-world device tracking data can be noisy; one way to handle this issue is to use point cloud registration techniques such as the iterative closest point registration [9] to align the points. Second, some points might not have accurate depth information; to ensure the reconstruction quality, only points with high depth confidence values, which measure the depth-map data's accuracy, should be used. Note that the point cloud will be updated based on newer view data; conceptually, such updates help deal with both spatial and temporal variance by initializing/overriding points in the 3D space at different times.
- *Step 3: Finalizing Environment Lighting.* The generated multi-view point cloud now consists of rich environment information and can be equated to having an enlarged virtual camera FoV at the rendering position. It is worth noting that enlarging the camera FoV at the observation position can also increase the camera observation coverage, though less effective than multi-view enlargement. In order to directly use modern rendering engines to support realistic rendering, the point cloud will be converted to lighting formats, such as spherical image format or environment map. For example, one can project the point cloud into a 2D environment map that captures the omnidirectional environment lighting.

3 MOTIVATION AND CHALLENGES

Spatial and Temporal Variance. Indoor lighting can be both spatially and temporally variant [24, 54, 65]. Rendering using lighting information from locations other than the *rendering position* could lead to potential

visual degradation. To demonstrate the impact of such variances on the rendering effect, we compare a virtual object rendered with the lighting information at the rendering position and at the *observation position* in Figure 3a. We can see that the mirror ball on the right has non-desirable visual effects, i.e., neither zoomed-in views contain the correct reflections of the chair and the table. Thus it is important to account for spatial variance when designing the reconstruction framework. It is intuitive to understand that lighting can change temporally even at the same rendering position. In this work, we handle the temporal variance by periodically reconstructing lighting.

Mobility-induced Noise. The inherent user mobility can naturally introduce noise to data required by the lighting reconstruction pipeline. For example, when a mobile user engages with an AR application, the user might move around, introducing measurement errors into the 6DoF tracking data or leading to blurred RGB images. Other factors, such as the mobile camera's position relative to the rendering position, can also impact the quality of camera observations. Both tracking and camera data are commonly used for lighting estimation [65, 66]. Figure 3b shows that the point cloud can have incorrect alignment when naively using two consecutive color and depth images. We note that misalignment is a commonly occurring error in current AR applications that uses ARKit's world tracking data [18].

Limited Sensing Capability. Mobile vision sensors have become more potent over the past few years, especially with the newly equipped depth-sensing capability. However, most commercial mobile cameras still have limited FoVs ($< 120°$) [5, 26], much less than the desired $360°$ cameras commonly used by the movie industry to reconstruct lighting information [38]. Furthermore, a large portion of modern phones still do not have access to depth sensors and rely on different algorithms to estimate depth [19, 64]. Depth estimation errors can significantly impact the 3D point cloud generation process. In short, the limited mobile sensing capability can make it challenging to capture high-quality data to use for lighting reconstruction.

Resource-quality Trade-offs. The task of generating high-quality environment lighting information can be very computation-intensive. Existing state-of-the-art lighting models that support visually coherent reflection often require running on a powerful GPU server to achieve reasonable performance [53]. With an additional setup of physical light probes, for example, GLEAM can take from 30ms to 400ms to update scene lighting estimation [47]. By sacrificing the lighting quality, Zhao et al. achieved real-time lighting estimation (20.1ms) with low-fidelity spherical harmonics coefficients [66]; Somanath et al. trained a deep learning model that can generate an HDR environment map in less than 9ms on newer iPhones but severely sacrifices visual coherence [52]. It is challenging to navigate the resource-quality trade-offs in providing visually coherent lighting.

4 LITAR DESIGN

4.1 Overview

We design LitAR to address the challenges mentioned above to reconstruct high-quality environment lighting information. LitAR is an adaptive framework that progressively, e.g., as AR users naturally move around the indoor environment, reconstructs environment lighting for any user-specified reconstruction positions. In contrast to prior estimation-based work [22, 39, 53, 65], the core of LitAR lies in how to effectively *reconstruct* environment lighting information from a sequence of limited camera observations. Our reconstruction-based approach has the promise of obtaining more accurate lighting information and achieving better visual effects without requiring expensive data collection, model training, or physical setup [47].

Specifically, LitAR proposes a novel *two-field lighting reconstruction* technique (§4.2) to produce geometrically accurate transformation to handle the challenge of spatial variance by transforming indirect scene observations to the desired lighting information. Figure 4 presents an overview of LitAR. To mitigate the impact of mobility-induced noise on the reconstruction quality, LitAR proposes two policies for guiding bootstrapped device

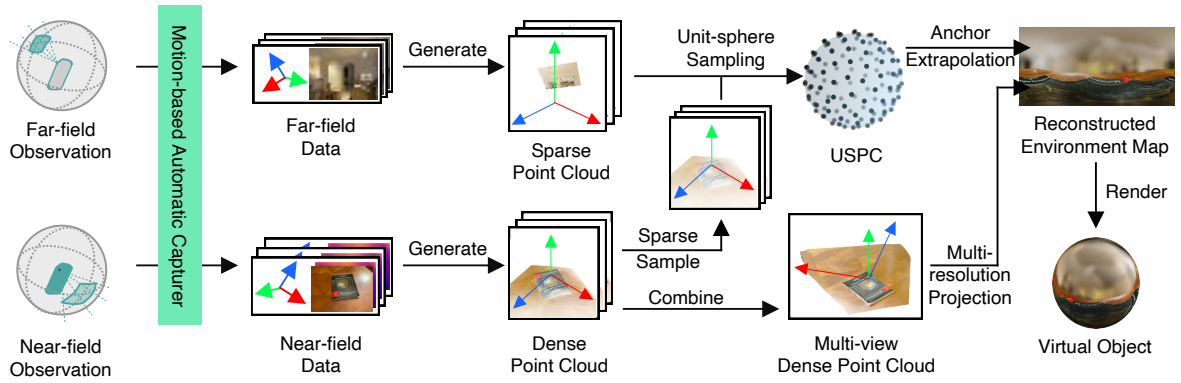

Fig. 4. ***LitAR's overview.*** LitAR separately reconstruct for the near-field (§4.2.1) and far-field (§4.2.2) regions from camera observations strategically guided and automatically captured. The near-field data, which has a higher impact on spatial variance and consists of more accurate depth information, will be used to generate a multi-view dense point cloud. The far-field data will be projected to color a unit-sphere point cloud (USPC) with the sampling technique from [66], then will be extrapolated to fill neighboring pixels in the environment map. Finally, the dense point cloud will be projected to multi-resolution environment maps, which will then be combined, using our *multi-resolution projection* technique (§4.4.1).

movement (§4.3.1) and automatically capturing required data based on motion (§4.3.2). To account for limited mobile sensing capability, LitAR only requires depth information on some camera observations (i.e., *near-field observations* that have the reconstruction position in the view) and applies point cloud registration to correct the device tracking errors (§4.5.2). The resource intensity is dealt with from the outset with a mobile-centered design: camera observations are divided to go through two separate execution branches to a multi-view dense point cloud and a fixed-size point cloud. This two-branch design effectively reduces LitAR's computation and memory consumption. LitAR proposes two novel performance optimization techniques, multi-resolution projection (§4.4) and anchor extrapolation (§4.4.2), and achieve the real-time environment map rendering at the edge. Many knobs can impact the lighting reconstruction quality and time; LitAR allows mobile AR developers to express such trade-offs via a configurable design (§4.5.1).

4.2 Two-field Lighting Reconstruction

At the high level, our two-field lighting reconstruction technique divides the task of lighting reconstruction into two sub-tasks: one task that leverages depth information to produce high-quality lighting from near-field observations and one lightweight task for reconstructing lighting from far-field observations. In other words, LitAR will generate two intermediate point clouds from camera observations for rendering environment maps. The *multi-view dense point cloud* is the outcome of judiciously applying the geometrically accurate transformation and dense sampling on near-field observations; the *unit-sphere point cloud* is the sampling outcome of the sparse point clouds from the far-field observations and the dense point clouds. Recall that we divide the camera observations into two types, *near-field observation* that includes the reconstruction position in the view and *far-field observation* that does not. As explained below, such division is based on the key insight that spatial variance has varying impacts on different camera observations.

Figure 5 illustrates the different importance of considering spatial variance, depending on the relative position of the interested pixel to the observation and reconstruction positions. To perceive any position P_{env} in the

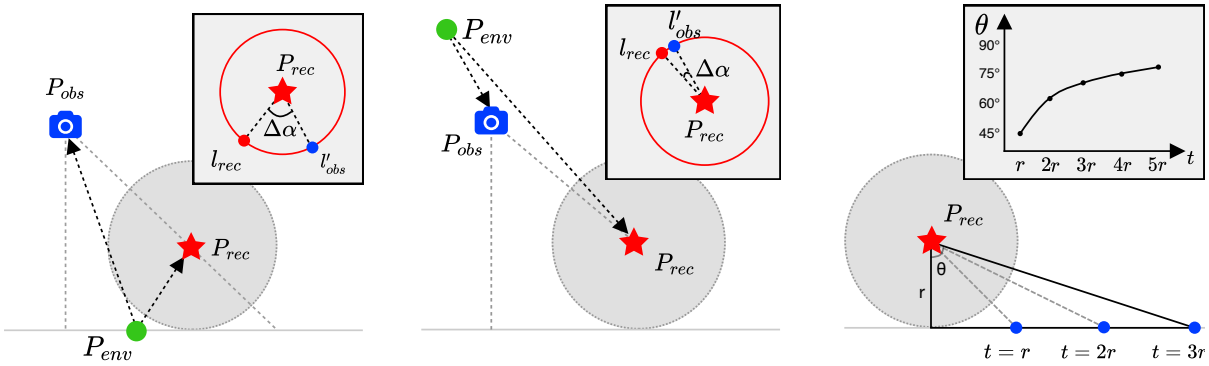

(a) Spatial variance in near-field **(b)** Spatial variance in far-field **(c)** Near-field boundary size

Fig. 5. ***Illustration of spatial variance impact.*** We visualize the near and far-fields observations in a 2D front view. P_{obs} and P_{rec} represents observation position and reconstruction position, respectively. l'_{obs} and l_{rec} represent the incoming light ray from an environment position P_{env} that are observed at P_{rec}. (a) & (b) It is more important to consider spatial variance for pixels observed in near-field than ones in far-fields, i.e., larger $\Delta\alpha$. (c) Increasing the near-field boundary size, e.g., from r to $2r$ vs. $2r$ to $3r$, has a diminishing impact on the reflection surface.

environment, one has to observe light emitted/reflected from P_{env}. As shown in Figure 5a, if the P_{env} is in the near-field, the reconstruction quality can be poor if we do not consider spatial variance. That is, l'_{obs}, translated directly from the l_{obs} observed at P_{obs}, can differ significantly (i.e., larger $\Delta\alpha$) from l_{rec} that should be perceived at P_{rec}. On the contrary, as shown in Figure 5b, if the P_{env} is in the far-field, l'_{obs} can be a good approximation for l_{rec} (i.e., much smaller $\Delta\alpha$). In short, far-field observations are impacted much less by spatial variance.

Other benefits of separating camera observations into near-field and far-field include better tolerance of limited mobile depth-sensing capability and resource efficiency. A naive alternative design of applying the same reconstruction pipeline to camera observations can lead to incorrect point clouds and demand resources proportional to the indoor scene space (i.e., the total number of points). In contrast, our design of processing far-field observations demands less memory and computation resources by using a fixed-size point cloud [66].

4.2.1 Spatial Variance-aware Near-field Reconstruction. To effectively transform camera observation(s) to the environment map at the reconstruction position, LitAR leverages the increasingly popular depth sensor in mobile camera system [31, 32]. Depth sensors enable the possibility of capturing geometrically accurate environment observations. First, we densely sample camera color and depth image buffers for each near-field observation. Then, the image buffers and the camera transformation matrix (rotation, translation) are used to generate the position and color of a dense 3D point cloud. Currently, we use the camera transformation matrix information provided by commercial AR frameworks. Such information is often referred to as device tracking data. The point cloud generation process can be time-consuming; to speed up this process, we first separate the position and color generation tasks and then execute both tasks on the GPU. Finally, the output point cloud position and color information (i.e., dense point cloud) are written to a global point cloud buffer that maintains a multi-view point cloud for the current reconstruction session.

To support multi-view reconstruction, LitAR uses a motion-based automatic capturing (§4.3.2) to supply the reconstruction pipeline with new near-field observation. LitAR assigns a unique indexing identifier for each near-field observation. This identifier is subsequently used for other data, including the camera transformation

matrix and the derived dense point cloud. The global point cloud buffer is updated with the least-recently-observed policy, i.e., the points associated with the oldest near-field observation will be replaced.

We define a *near-field boundary* as a constrained cubic space that contains the points belonging to the near-field observations that will undergo further processing. That is, for points that are outside the near-field boundary, we will not perform multi-resolution projection (§4.4.1). Theoretically, this boundary can be as big as the indoor scene. However, having a too large boundary can have undesirable implications on both the memory and computation consumption and is often unnecessary. Figure 5c shows that increasing the near-field boundary size has a diminishing impact on the reflection surface. For example, increasing the boundary from 2X to 3X of the virtual object size only increases the coverage by 8.13°, a 1.13X. In short, we use a configurable near-field boundary to trade-off the resource consumption of the near-field observation processing and reconstruction quality for different virtual objects. We set the near-field boundary side length to two meters based on the AR virtual objects we use for testing. It is worth noting that AR developers should adjust this boundary accordingly for large virtual objects or divide the large object into smaller objects to have multiple reconstruction positions. The dense near-field point cloud generation allows us to produce geometrically accurate camera observation transformations and produce continuous lighting representations.

Our spatial variance-aware observation transformation still generates an approximated observation at the reconstruction position due to the lighting variance from different observation directions. We currently assume that the light does not change between different observation directions, which serves the mobile AR rendering purpose in most cases. However, such an assumption may lead to visually incorrect results if the environment around the reconstruction position contains reflective physical objects, e.g., mirrors. It is possible to further address such concerns by meticulously selecting light ray directions between observations, which we leave as part of future work.

4.2.2 Directional-aware Far-field Reconstruction. Mobile depth sensors usually only capture surrounding environment depth in a limited range. For example, the LiDAR sensor on iPhone 13 Pro can sense depth up to 5 meters [51]. Thus, it might not be suitable for sensing large physical environments. However, the desired environment lighting for AR rendering varies directionally depending on the surrounding physical world environment. To address the directional variations, i.e., the anisotropy property of environment lighting, LitAR reconstructs far-field lighting by sparsely sampling camera observation to provide omnidirectional lighting.

Even modern cameras have relatively small FoVs, thus capturing only a small portion of the environment covering limited directions. However, reconstructing a dense point cloud to address the anisotropic lighting property from far-field observations is impractical as generating a dense point cloud for a far-field environment can be potentially unconstrained in terms of computation and data storage. Additionally, objects in the far-field observations may exceed the range limitation of mobile depth sensors, which makes geometrically accurate transformation difficult. The inherent nature of the far-field environment thus leads to lower confident far-field depth observations, which makes it ill-suited for dense point cloud reconstruction.

We design a lightweight process to reconstruct far-field lighting from sparsely sampled camera images to address these limitations. Recall that a camera observation is considered a far-field observation if the reconstruction position falls outside the camera view. For a far-field observation, we sparsely sample a low-resolution camera image and obtain the current camera transformation matrix, similar to §4.2.1. Note that we do not capture depth data for the far-field observation as its depth information may be inaccurate, and the spatial variance less impacts it. To generate the sparse point cloud, we assume the depth of all pixels to be one and scale the camera intrinsic values accordingly. We use a similar design to [66] by projecting the sparse point cloud to a set of uniformly distributed anchor points on a sphere, called *USPC*. As demonstrated in prior work [66], the design of USPC is aware of directional lighting variance and thus addresses the anisotropy property of environmental lighting. In this work, we set the number of anchors of the USPC to 1280. The anchor points are colored by

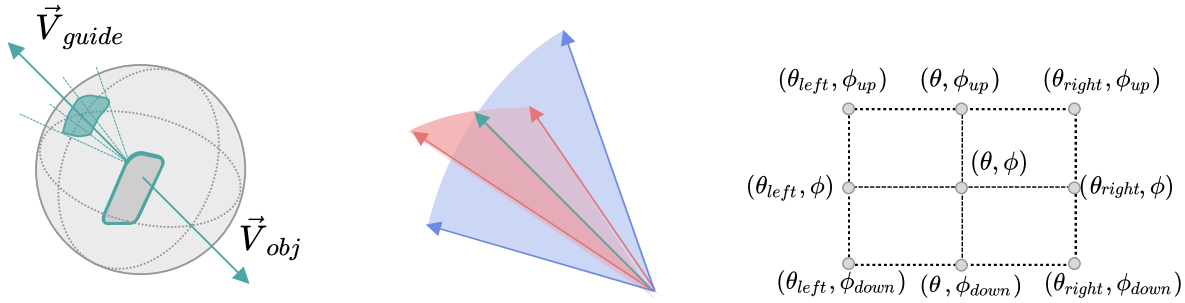

(a) Front & back facing observations **(b)** Horizontal & vertical movement **(c)** Movement direction grid

Fig. 6. ***Guided bootstrapped movement.*** Our guided bootstrapping movement technique directs users to point the mobile camera toward the opposite direction $\vec{V}_{guide}$ of the virtual object viewing direction $\vec{V}_{obj}$, and rotate along horizontal and vertical directions to increase the far-field observations. The movement follows a grid-style pattern, where (θ and ϕ) denote the observation direction, in spherical coordinates, for each movement.

combining the color data from the sparse point cloud and ambient light sensor readings. Recall that we want to use USPC to represent the lighting from all directions, including near-field observations. Therefore, we sparsely sample the dense point cloud generated from the near-field observation; then, the resulting sparse point cloud is similarly projected to the same USPC. In short, the reconstructed far-field lighting is represented as a unit-sphere point cloud with a much smaller memory footprint (proportional to the anchor size) while still providing good directional-aware lighting support.

4.3 Noise-tolerant Data Capturing Policies

4.3.1 Guided Bootstrapped Movement. Another key design of LITAR to reconstruct high-quality lighting is to better exploit user movement, a distinct feature of mobile AR. We observe that commercial mobile AR frameworks such as ARKit have built-in support for explicitly guiding mobile AR users to scan their physical surrounding environment before using the app. Note such practice is often used for calibrating world tracking data, but not for lighting estimation [4]. However, this commonly adopted movement practice often leads to a biased sample of environment lighting in concentrated observation directions. This biased sample is due to the narrow focus on increasing the nearby environment's observation around the reconstruction position. Although commercial frameworks also use estimation models to estimate environment lighting from observations, such biased observations create a barrier to more accurate estimation. As we will show in §6.2.3, simply increasing observations with the common practice shows little improvement on rendering results.

Instead, we propose a novel yet simple guided movement policy to look at the *backward environment*, i.e., observable from the opposite direction to the virtual object viewing direction. This guided movement is designed to increase the observation directions rather than the observation overlapping and to help address the anisotropic property of lighting. In other words, our guided movement policy provides bootstrapping data at the AR application startup time to increase the far-field observations. As illustrated in Figure 6, our policy guides a user to look at the backside of the intended virtual object observation direction. We use a grid-style pattern to partition the observation directions and provide guided viewing directions for the user. Specifically, as shown in Figure 6c, the optimal choices on the number of observations could be $\{1, 3, 5, 9\}$ based on the horizontal and vertical direction partitions. The number of observations corresponds to the combination of moving *left* and *right* in horizontal direction, and *up* and *down* in vertical direction. We currently use an angular difference of 30

degrees in both horizontal and vertical directions. Furthermore, as our far-field reconstruction method does not reconstruct detailed observations, our guided movement can be performed without the user focusing on each camera observation orientation for a long time. In § 6.2.4, we will show that using the guided movement, LitAR can find more accurate color tone for filling unseen area and produce more accurate renderings.

4.3.2 Motion-based Automatic Capturing. Continuously capturing all camera observations or relying on the mobile AR user to manually capture them can lead to poor usability, low-quality data (e.g., images with motion blur), and high mobile resource consumption. For example, prior work has demonstrated that motion blur is a common occurrence in mobile AR—which we also observe—and can lead to low AR task accuracy [40]. Additionally, a recent low-frequency lighting estimation framework has demonstrated that strategically skipping the capture of specific camera frames has little impact on the estimation accuracy [66]. With the goals to provide good usability, capture high-quality data, and reduce resource consumption, we design a *motion-based automatic capturing* technique that leverages multi-sensor data to automatically select camera frames and AR data for lighting reconstruction. In a nutshell, this technique will only capture new observation data, both spatially (i.e., by checking device position and rotation information) and temporally (i.e., by updating a previously captured frame with the same device information).

Specifically, LitAR uses a simple timer-based policy to periodically assess the need to capture new data by checking if the mobile device has exhibited significant movement. In this work, we leverage the device accelerometer and gyroscope sensors to maintain a moving window of the device's most recent K position and rotation information (i.e., 6DoF). Every C milliseconds, LitAR will compare the current frame's device 6DoF information to the ones from the moving window to assess the likelihood of motion blur. If the device pose has changed for more than 10cm and 10°, the device is considered to have significant movement in a short time window, and the current frame is skipped. LitAR will re-run the check every frame until a new frame is found while the device is relatively stable. Otherwise, the current frame is captured. The timer will be reset once a new frame is captured in both cases. In essence, our motion-based automatic capturing will produce new data at least every C milliseconds, depending on the mobility. Both the moving window and capturing frequency can be configured, and in this work, we set $K = 5$ and $C = 300$.

4.4 Real-time Environment Map Rendering Techniques

Thus far, our two-field lighting reconstruction has generated two intermediate point clouds. To support high-quality multi-view lighting reconstruction for mobile AR, we need to convert the point cloud presentation to a lighting representation commonly supported in modern rendering engines. In this work, we choose *environment map* as the final lighting representation, which the mobile rendering engines can directly use. At the high level, to generate a high-quality environment map (i.e., visually continuous pixels) from a point cloud that consists of discrete points, one often needs to handle occlusion and inter-point connection. One common way to recreate the inter-point connections and calculate occlusion is to resort to conventional 3D reconstruction methods, e.g., Ball-Pivoting surface mesh reconstruction-based algorithms [8]. However, such a method is ill-suited for real-time applications as surface mesh reconstruction can be computationally intensive, e.g., we observe that it takes about 3 seconds to perform mesh reconstruction on a five-view dense point cloud. In this section, we describe two novel techniques called *multi-resolution projection* and *anchor extrapolation* for generating near-field and far-field portions of the environment map in real-time.

4.4.1 Multi-resolution Projection. We propose a lightweight technique called multi-resolution projection to convert the near-field dense point cloud to the respective portion in the environment map. In this work, we use the common equirectangular format to present the environment map. At the high level, multi-resolution projection projects a point cloud into a set of environment map images with decreasing resolutions and addresses the

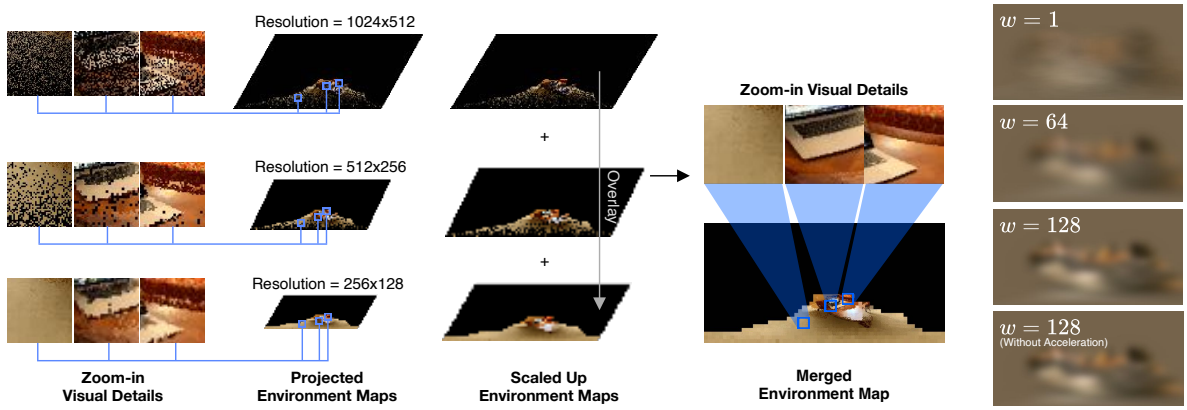

(a) Multi-resolution projection **(b)** Anchor extrapolation

Fig. 7. ***Illustration of multi-resolution projection and anchor extrapolation.*** (a) We show an example of multi-resolution projection with three resolution levels. The dense point cloud will be projected three times. The higher projection resolution leads to more visual details but has more discrete pixels; the lower projection resolution has more continuous pixels but fewer visual details and exhibits pixelation. We obtain a high-quality final environment map by scaling and overlaying each intermediate environment map. (b) We show that larger w leads to a less blurry environment map and that our nearest-anchor acceleration has minimal visual impact.

inter-point connection and occlusion at the 2D-pixel level. When projecting a point cloud onto one environment map image, multi-resolution projection first converts the point cloud's position from the Cartesian coordinate system to the Spherical coordinate system. Then, for each point, we calculate its 2D projection coordinate on the environment map based on the angle values of the point's spherical coordinate. Then, we assign the point cloud color to the corresponding pixel on the environment map. As multiple points can be projected to the same pixel of the environment map, for each pixel, we handle the point occlusion by selecting the shortest-distant projected point to color the pixel. Figure 7a illustrates an example of three-level resolution projection.

However, when the point cloud density is low, e.g., due to low capturing resolution, projecting point cloud only onto one environment map image resolution may lead to undesirable visual quality. For example, it might result in an image with discretely projected points rather than a continuous view of the scene, and it might not adequately represent the inter-point occlusion. We assign different size values for projected points through multi-resolution image projection to address these issues. We first project the point cloud into a series of images with decreasing resolutions; then, we scale all the projected images to the largest resolution via the nearest pixel interpolation after projection. Finally, the multi-resolution projection results are merged into a single environment map by selecting the shortest-distant projected point to the reconstruction position from each projected image per pixel. If multiple projected projects have the same distance, we select the one from the highest projection resolution as it has more visual detail.

We note that both the number of resolution levels and per-level resolution can be adjusted for different combinations of dense point clouds and reconstruction positions. However, our design of near-field boundary described previously in §4.2.1 suggests that all reconstructed near-field dense point clouds will be confined to a cubic space. Thus, it is possible to have a relatively fixed configuration to handle various scenes. In this work, we choose two resolution levels with per-level resolution as 1024x512 and 512x256, unless otherwise specified.

4.4.2 Anchor Extrapolation. Recall that by now, our two-field lighting reconstruction has generated a colored unit sphere-based point cloud (USPC) for the far-field lighting. To generate the corresponding environment map (in equirectangular format), we will use the anchor points to color each environment map pixel. However, the USPC, by design, only has a fixed number of anchor points; therefore, directly projecting anchor points to the environment map is likely to lead to a large number of empty pixel values. To address this problem, we design the *anchor extrapolation* technique that calculates each pixel value as a weighted average of USPC anchor values. This technique, in essence, assigns color value to pixels by extrapolating from their nearby anchor colors and will result in a gradient coloring and blurring effect.

Specifically, we first initialize each pixel of the environment map with a normal vector, i.e., a unit vector from the sphere center to the pixel position. This is because a pixel in the equirectangular format of an environment map can be easily presented in the Spherical coordinate system. We then calculate the i^{th} pixel color c_i using the following equation:

$$c_i = \frac{2}{N} \sum_{j=1}^{N} max(\vec{p}_j \cdot \vec{n}_i, 0)^w c_j. \quad (1)$$

Where $\vec{n}_i$ represents the pixel normal vector, N is the number of anchors, p_j and c_j are the normal vector and color for the j-th anchor. Note that the dot product between $\vec{p}_j \cdot \vec{n}_i$ is effectively the cosine value of the angle between these vectors, as $|\vec{p}_j| = |\vec{n}_i| = 1$. The *max* function effectively filters out all the anchor points in the hemisphere opposite to the i^{th} pixel. Further, w is an exponent controlling the blurring level of far-field reconstruction; logically, a smaller w value will lead to more anchor points being used for the pixel calculation. Visually, a smaller w value will result in a more blurred environment map, while a larger w will produce a clearer environment map, as demonstrated in Figure 7b. In this work, we set w to be 128.

Note that calculating the pixel color using Equation (1) can be time-consuming as the weighted average has to iterate through all anchor points. However, we note that anchors do not contribute equally to the pixel color calculation. Intuitively, an anchor j that has smaller $max(\vec{p}_j \cdot \vec{n}_i, 0)$ decreases more quickly with the power w. Such anchors are also farther away from the pixel of interest than anchors with larger $max(\vec{p}_j \cdot \vec{n}_i, 0)$ value. In fact, we find that when $w = 128$, only 32 nearest anchors out of the 1280 contribute significantly (i.e., $max(\vec{p}_j \cdot \vec{n}_i, 0) > 0.1$). Thus, to speed up the pixel color calculation, we precompute the 32 nearest anchors for each pixel and their respective cosine values. This effectively reduces the number of anchors by about 40X and allows the use of cached results for the weighted average calculation. Figure 7b shows that our acceleration has minimal visual impact.

4.5 LitAR Quality-Performance Configurations

4.5.1 Reconstruction Session Settings and Initialization. LitAR uses *lighting reconstruction session* to manage each multi-view reconstruction task. A lighting reconstruction session has the same lifecycle as its corresponding virtual object; the session is created when a virtual object placement request is issued and is destroyed when the placed object is removed from the scene. As AR applications might need to support multiple virtual objects in the view, LitAR thus supports multiple active lighting reconstruction session per AR session (i.e., during the AR application's lifetime). At the beginning of each session, LitAR collects static device-specific information, e.g., camera intrinsic, current ambient lighting data, and camera image native resolutions, to bootstrap subsequent lighting reconstruction operations.

LitAR supports configuring a number of knobs, including color image sampling rate, number of views, multi-resolution projection resolution levels, and environment map size, that trade-off visual quality and reconstruction performance. These knobs can be categorized into three types, i.e., data capturing, two-field lighting reconstruction, and environment map rendering. Thus, each session's startup latency and subsequent near/far-field reconstruction

depend on the specific configurations. LitAR users (e.g., mobile AR developers) can configure each lighting reconstruction session based on application performance requirements or select one of the three presets: low, medium, and high. In §6.1.2, we show that all presets achieve better visual quality than ARKit and take an increasing amount of time to generate an environment map.

4.5.2 Point Cloud Management. To achieve low-latency point cloud operations, LitAR leverages the edge to generate, manage, and transform both the sparse and multi-view dense point clouds. To exploit the inherent parallelism of point cloud operations, LitAR performs these operations on the GPU device. However, even with unified memory, the managed memory still must be copied to the GPU memory (by the driver) when the GPU accesses them. If not careful, we can still encounter expensive GPU memory access overhead. Thus, we carefully design the memory layout using a continuous memory buffer to store the multi-view dense point cloud and a fixed number of anchor points. When new view data is processed, LitAR overwrites the point cloud memory buffer by replacing the oldest data (to support temporal variance) or replacing the data with the same view identifier (to support spatial variance). This fixed-view design keeps the memory layout unchanged, thus avoiding paging setup overhead while still producing high-quality environment maps.

Additionally, LitAR includes an asynchronous point cloud registration to address the mobility-induced noises which can lead to misaligned point positions. In other words, LitAR runs point cloud registration in parallel to the main two-field lighting reconstruction and will update the environment map with the aligned point cloud once the registration completes. We note that the point misalignment is largely due to the inaccurate device tracking data provided by the AR framework, in this case, ARKit. Providing accurate device tracking information is an important but orthogonal research question; prior work such as ORB-SLAM2 [44] and Edge-SLAM [7] can achieve good tracking in about 26ms-50ms. In this work, we use the iterative closest point registration [9] to mitigate the impact of noisy tracking data on the lighting reconstruction. During our preliminary study, point cloud registration is not always needed (e.g., when mobile AR users are relatively static) and can take significantly longer than other operations (e.g., 200ms for handling five 1024x768-point views). Currently, the point cloud registration is off by default.

5 IMPLEMENTATIONS

We implement all the techniques described in §4 in a prototype system called LitAR (§5.1). For facilitating controlled experiments, we also develop an Unreal Engine-based mobile AR simulator (§5.2).

5.1 LitAR Edge-based Prototype

We implement LitAR in C# and Python with 2.2K lines of code. Figure 8 shows an architecture overview of LitAR. LitAR consists of two logical modules: the client-side that captures, encodes, and sends the data necessary for the lighting reconstruction sessions, and the edge-side that decodes the keyframe data, generates intermediate point clouds and renders the environment map. LitAR currently supports AR applications built with Unity3D [61] and AR Foundation [60] framework.

Client-side. The client module of LitAR is implemented as a Unity package. We provide an entry script *ARLightingReconstructionManager* as a *MonoBehavior* subclass to allow the developer to supply system configurations and visual quality-related information through the Unity editor UI. *ARLightingReconstructionManager* also manages the memory usage and function calls of all lighting reconstruction sessions in an application's lifecycle. We implement the *motion-based automatic capturer* by leveraging the AR device tracking data provided by AR Foundation to automatically capture environment data that will not be subjected to the camera motion blurs. We directly perform the nearest neighbor sampling on the device's native color and depth image data for the visual data. Specifically, for the AR application running on our testing device iPad Pro, we sample color and depth images with the format of YCbCr 4:2:0 and float32, respectively. The captured color and depth images are

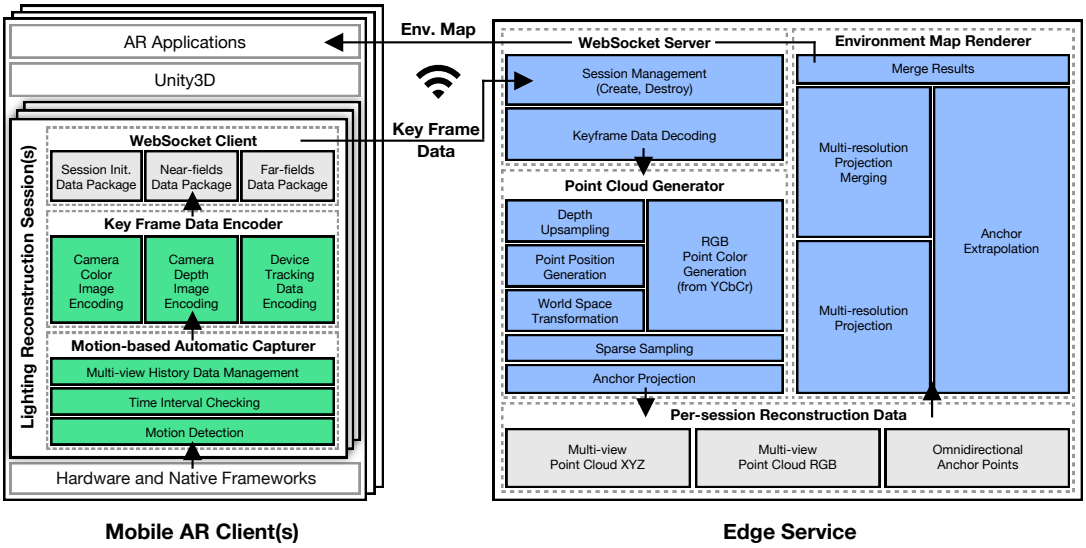

Fig. 8. ***A system architecture overview of LitAR.*** The framework provides high-quality lighting in the form of an environment map for mobile AR applications with two logical components: client-side and edge service. LitAR can support lighting for multiple reconstruction positions per AR session on the client side and allows multi-user scene data sharing via the edge service.

then encoded with a 1-byte unique package identifier and device tracking information into three different binary data packages, including the session initialization, near-field, and far-field. We refer to these data packages as *keyframe data*. LitAR manages a WebSocket session for low latency communication with the edge server, i.e., sending keyframe data and receiving environment map.

Edge-side. On the edge server, we implement a Tornado-based[57] WebSocket service to communicate with the client. The WebSocket server dispatches the package to different operations for each received binary data package based on its package identifier. We leverage NumPy [29] to decode and convert the received binary packages into different data types and structures. To improve the performance of point cloud-related operations, we implement these operations, including point cloud generation, multi-resolution projection, and anchor extrapolation in CUDA kernels using the Numba library [37]. As such, these operations run on the edge GPU. In our edge system memory management, we also leverage the unified memory [13] to avoid time-consuming data copying between CPU and GPU. Our edge server implementation can also fall back to traditional GPU memory without any modification to support other GPU hardware that does not have unified memory.

Mobile-edge Communication. We design a tailored low overhead and compact networking communication scheme to support the low-latency lighting reconstruction goal. Both near and far-field data are serialized into binary formats. Specifically, we stream only the device's native color and depth data for near-field data and reconstruct the point cloud on edge. Compared to directly streaming float32-encoded point cloud in the XYZRGB format, we need at most 22.9% of the bytes. Also, as we only capture sparse camera images during far-field reconstruction, the far-field keyframe data is significantly smaller than near-field keyframe data (41473 bytes vs. 270401 bytes).

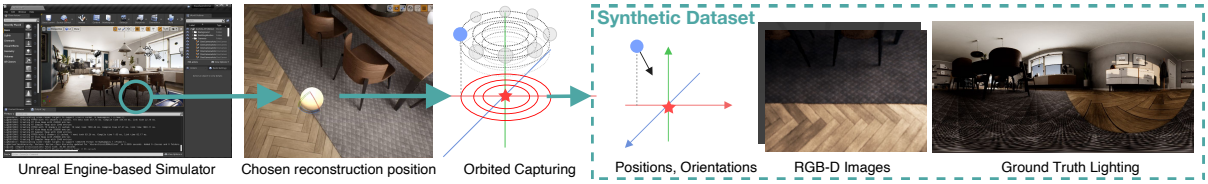

Fig. 9. ***Unreal engine-based simulator and synthetic dataset generation process.*** We generate an indoor synthetic dataset using Unreal Engine-based simulator. At each manually chosen positions, we use an orbit trajectory to build observations around the chosen position and place virtual camera to capture camera images. We extract camera positions, orientations, RGB-D images, and ground truth environment map.

5.2 Unreal Engine-based mobile AR simulator

We implement a mobile AR simulator by leveraging a high-fidelity 3D graphics rendering engine, Unreal Engine [21]. Figure 9 presents the simulator workflow. First, we use Unreal Engine 4 to create a photorealistic indoor scene based on the *ArchViz* project [50], a high-quality architectural visualization for interior design. Other photorealistic scene assets can also be used. Next, we create a virtual camera using the Blueprint programming system that takes controlled variables to modify the camera's movement and internal properties, e.g., FoV. As such, we can simulate device/user movement by controlling a virtual camera movement in a photorealistic 3D indoor scene. Finally, we can configure the simulator with desired variable values to generate a synthetic dataset for rendering purposes, including camera observations and environment physical properties. Our simulator can be extended to support future studies and bears the following advantages over a device-based setup: *(i)* our simulator makes it easier to extract high-quality environment lighting and physical information to serve as the ground truth. At the same time, it can be expensive or unpractical to obtain such information due to physical limitations on measurement and observation. *(ii)* it is easier to study individual factors in isolation by applying controlled changes to the scene environment and simulated mobile devices.

AR Virtual Object Rendering. We develop a browser-based renderer using the Three.js rendering framework [56] to automate the process of rendering virtual objects of interest. Specifically, our renderer uses information, including reconstructed lighting, the camera position, and properties, from our synthetic dataset to render a 3D virtual object at the resolution of 1024x768. The renderer then trims empty pixels outside rendered objects to remove the object-to-frame size impact on PSNR calculation when using different camera FoV settings. The resulting images of rendered objects serve as the basis for comparing different lighting reconstruction methods.

6 EVALUATION

We evaluate the performance of LitAR using both a lab testbed and the simulator. The lab testbed includes a LiDAR-enabled iPad Pro serving as the client and a Jetson Xavier NX [45] board serving as the edge server. The iPad and the Jetson board communicate via a resident WiFi with an average of 7.08ms (± 3.31ms) latency and 508Mbits/sec (± 12Mbits/sec) bandwidth. For testbed-based experiments, we choose three different indoor scenes and compare LitAR with three different baselines: *(i)* ARKit 5 [34], a commercial AR framework developed by Apple, and we use its Environment Probe [33] feature to generate environment maps; *(ii)* LitAR with *point cloud registration* turned on; *(iii)* LitAR with *mesh reconstruction* instead of the lightweight multi-resolution projection module. Note that ARKit's lighting estimation feature is backed up by the EnvMapNet [52]. We measure both the reconstruction time and visual quality for all methods. For the quantitative visual quality comparison, we use Peak signal-to-noise ratio (PSNR) and Structural Similarity Index (SSIM). Each method's PSNR and SSIM values are calculated by comparing the rendered virtual object to the physical object. In this work, we use the classical

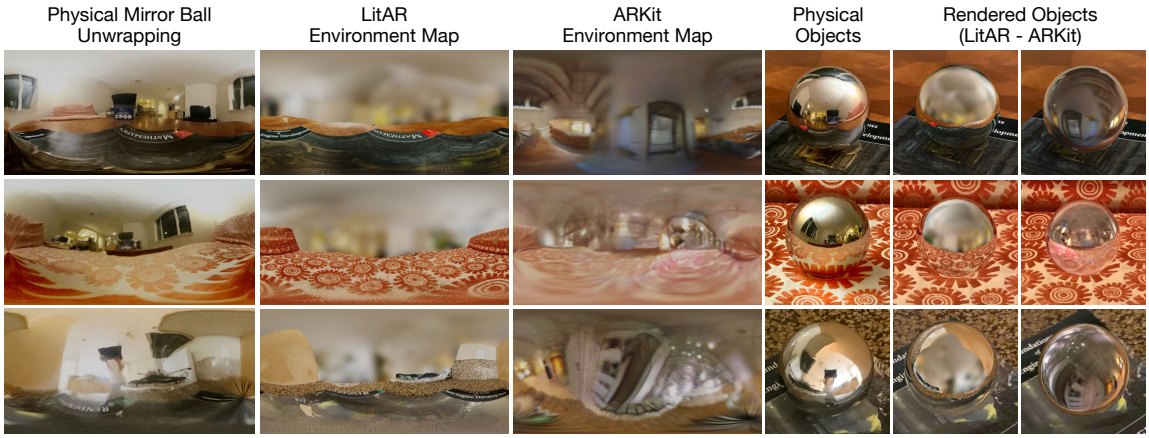

Fig. 10. ***LitAR rendering visual effect comparison.*** Each row represents an indoor scene. *Column 1:* the panorama view of a scene at the reconstruction position by unwrapping the physical mirror ball reflection [15]. *Column 2:* LitAR's environment maps have good visual detail and quality of the near-field portion while largely maintaining the structural similarity to the corresponding physical scene. *Column 3:* ARKit's environment maps show varying performance, sometimes completely different from the scene (row 1), while others with less visual details.

physical mirror ball as it can be easily acquired. For both PSNR and SSIM, the higher the value, the better the visual performance.

We use the simulator to evaluate LitAR's performance in a wider range of scenarios. Our simulator allows easy ground truth lighting information extraction at any reconstruction position from a photorealistic 3D indoor scene. For simulation-based evaluations, LitAR is evaluated with six objects of different shapes and materials and is compared to two baselines: *(i)* using a 360° camera at the observation position, akin to [58]; and *(ii)* Xihe, a recent academic framework that produces real-time low-frequency lighting estimation from RGB-D images [66]. We describe the synthetic dataset used in our study in §6.2.1.

To provide an in-depth evaluation of LitAR's performance, we also conduct a number of ablation studies that demonstrate the quality-performance trade-offs (§6.1.2) and highlight our design choices for near and far-field reconstructions and identify applicable scenarios (§6.2.3 and 6.2.4). The three quality presets for near-field reconstruction are configured as following: *(i)* LitAR (low): number of views is 3, color image resolution is 256x192, multi-resolution projection resolutions are [512x256, 256x128, 64x32], environment map resolution is 512x256; *(ii)* LitAR (medium): number of views is 4, color image resolution is 512x384, multi-resolution projection resolutions are [768x384, 384x192], environment map resolution is 512x256; *(iii)* LitAR (high): number of views is 5, color image resolution is 1024x768, multi-resolution projection resolutions are [1024x512, 512x256], environment map resolution is 1024x512. All three presets for far-field reconstruction have the color image resolution of 32x24 and share the same environment map resolution configurations as near-field.

6.1 LitAR Testbed-based System Performance

6.1.1 End-to-end Evaluation. We compare the end-to-end rendering visual effects and the runtime performance of LitAR and ARKit. As shown in Figure 10 (last two columns), virtual mirror balls rendered with LitAR have more reflection details and overall better color tune than ones rendered with ARKit's learning-based method. Concretely, for all three scenes, LitAR's virtual balls have higher visual similarity to the same-sized physical

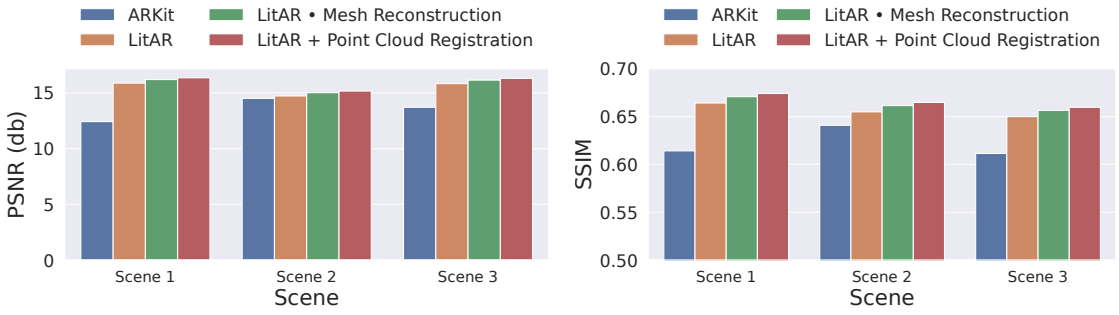

(a) PSNR comparison **(b)** SSIM comparison

Fig. 11. ***LitAR visual quality comparison.*** LitAR outperforms ARKit for all three real-world scenes. Further, using the conventional mesh reconstruction in place of our lightweight multi-resolution projection only increases the PSNR/SSIM values slightly by 2%/1%. Similarly, turning on the asynchronous point cloud registration has only minor improvement by 3%/1.5%. Recall that mesh reconstruction and point cloud registration can take a few seconds (§4.4) and a couple hundred milliseconds (§4.5.2), respectively. In short, LitAR achieves the best quality-performance trade-off.

mirror balls. In contrast, ARKit's virtual balls either reflect incorrect indoor scenes (especially on the far-field portion of the environment) or lack fine-grained visual details, e.g., the text from the book cover. Such visual quality differences can be more easily observed by comparing the generated environment maps (columns two and three) to the unwrapped images from the physical mirror ball. Note that the unwrapped images do not represent the ground truth lighting as they are often distorted but can serve as a visual guide of the panorama view at the reconstruction position. By comparing the environment maps generated by LitAR to the unwrapped images, we see that LitAR can reconstruct highly accurate scene elements from near-field observations while recovering similar environmental geometry and color tone information from far-field observations.

Figure 11 quantifies the visual quality with two commonly used image metrics. Both PSNR and SSIM are calculated by comparing the rendered object to a physical mirror ball image at the same reconstruction position. We see that LitAR outperforms ARKit on all three real-world captured scenes, with up to 14.3% higher PSNR and 5.5% higher SSIM. When replacing our lightweight multi-resolution projection component of LitAR with the Ball-Pivoting surface mesh reconstruction [8], we only notice a minor increase in the PSNR/SSIM values. This observation demonstrates the effectiveness of multi-resolution projection for generating high-quality near-field reflections. Similarly, we do not observe significant improvement when running LitAR with the point cloud registration component. We suspect this is because AR frameworks such as ARKit can provide reasonable device tracking data for most cases with low movement speed. We observed that ARKit's tracking data often drifts for faster movement use cases, which makes the point cloud registration component an integral one. As both of the LitAR's variations do not show noticeable visual quality differences to LitAR, we omit their visual effect comparisons.

Finally, the end-to-end reconstruction latency of near-field/far-field takes on an average of 134.4ms/57.5ms, respectively. Detailed component-wise time breakdown is discussed in the next section. These latencies translate to updating high-quality lighting roughly at 22fps, i.e., every 134.4ms LitAR can provide one near-field and two far-field environment maps. Such update frequency should be sufficient for most AR applications [62, 63]. For AR applications that require higher update frequency, we can either resort to more powerful edge servers (currently using an energy-efficient Jetson board) or use a lower quality setting, as discussed in the next section.

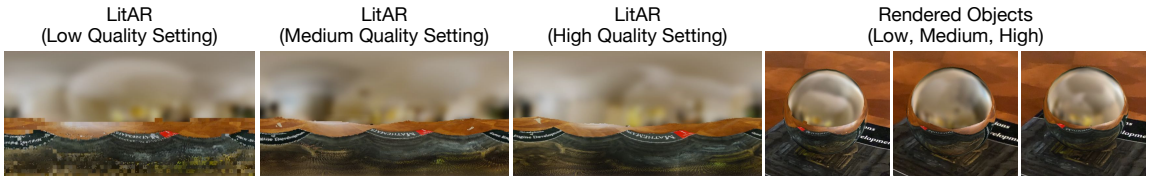

(a) Rendering visualization on different quality presets

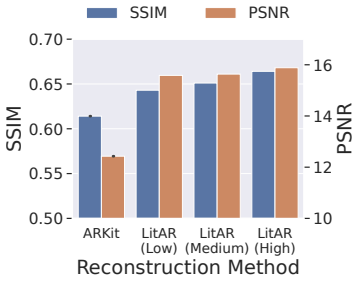

(b) Visual quality comparison

System Component	Near-field (ms)			Far-field (ms)		
	low	Medium	High	low	Medium	High
Data Encode	5.11	15.01	50.13	0.18	0.18	0.18
Data Offload	4.07	7.78	18.24	0.55	0.55	0.55
Dense Point Cloud Generation	8.39	9.71	15.62	N/A	N/A	N/A
Multi-resolution Projection	9.02	9.89	14.56	N/A	N/A	N/A
Sparse Point Cloud Generation	N/A	N/A	N/A	0.03	0.03	0.03
Anchor Extrapolation	N/A	N/A	N/A	19.03	20.32	21.72
Environment Map Download	20.01	29.11	35.83	20.02	29.71	35.03
End-to-end Reconstruction	46.6	71.5	134.38	39.81	50.79	57.51

(c) Reconstruction latency

Fig. 12. ***LitAR rendering quality-performance trade-offs.*** We show the time breakdown for LitAR to generate a near-field and far-field environment map. All quality settings achieve better SSIM than ARKit. A large portion of time, at least 26.46%, was spent on edge-related operations (data encode/offload and environment map download). This observation suggests that LitAR has the promise to deliver high-quality environment maps directly on the device as mobile device GPU becomes more powerful.

6.1.2 Rendering Quality-performance Trade-offs. We compare the rendering quality and latency of LitAR under different presets. Figure 12a shows the rendering visual effects. We note that environment maps generated at all three settings provide visually coherent near-field reflection and anisotropic correct far-field color tone. We can observe some pixelation on both the environment map and the rendered mirror ball object for the low-quality preset due to low capturing resolution. When comparing the PSNR and SSIM values, all three settings achieve better quality than ARKit. For example, the low-quality preset has a 4.5% higher SSIM value than ARKit. Moreover, the visual quality difference among the three presets is minimal, with only up to 3.5% between low and high quality.

Further, we measure the time breakdown of LitAR's near-field and far-field reconstructions. Table 12c shows the average performance over three runs. For near-field reconstruction, each component's time increases with the quality setting. For example, the time to encode the camera observations sees similar increases as the capturing resolutions, about 10X with 16X more pixels. We note that at the high-quality setting, the total time to encode and upload data takes 68.4ms, about 1.9X of the environment map download time, even though the upload/download resolution ratio is 1.5X. In contrast, at the medium-quality setting, with the same upload/download resolution ratio, it is 21.7% faster to encode and upload data than downloading. This observation is because we are uploading device data in the format of YCbCr 4:2:0, which has a smaller data size than the RGB environment map under the same resolution. Note that we are sending back the uncompressed RGB environment map for quality consideration. This observation suggests an interesting trade-off presented by the data encoding scheme in a real-world deployment. Moreover, this result also demonstrates that network-related operations (an artifact of using the GPU-based edge device) take up most of the end-to-end time, at 62.6%, 72.6%, and 77.5% for low, medium, and high quality,

respectively. The network performance bottleneck suggests the immediate performance gain by directly using mobile GPU to run the entire reconstruction pipeline.

Far-field reconstruction observes a similar but slower upward increase in total time with the quality presets. In particular, the time to decode and offload image data and generate a sparse point cloud is the same for all three quality presets. For all presets of far-field, LitAR downsamples the native camera color image from 1920x1440 to a fixed 32x24 resolution. The anchor extrapolation and environment map downloading time increase slightly with the environment map size. To put the latency performance of LitAR in context, we note that a recent physical probe-based framework requires 30ms-400ms to generate environment map [47]. To understand the ARKit's performance, we use the inference time of its underlying deep learning model EnvMapNet [52] as ARKit does not expose APIs to measure the end-to-end environment map generation. Even though the EnvMapNet model can run in 9ms, as reported by Somanath et al., we have shown previously that its visual quality is often lacking compared to LitAR. Moreover, the total time for ARKit to generate an environment map is likely to be similar to LitAR if accounting for other necessary steps, including data capturing and memory copying. In short, this detailed breakdown analysis demonstrates that far-field reconstruction can achieve near real-time for all presets; when used in conjunction with near-field reconstruction, the mobile AR applications can receive a sufficient number of environment map updates.

6.2 Simulation-based Performance Evaluation

6.2.1 Synthetic Dataset Generation. We describe the methodology we follow to use our simulator to generate the synthetic dataset for our evaluation (see Figure 9). In the created indoor scene, we first manually choose ten reasonable positions to be considered as lighting reconstruction positions for placing virtual objects. Example reconstruction positions include on the floor or table. We vary several factors for each reconstruction position, including the number of capturing positions, mobile user/device height, and observation distance, to generate 72 camera observations. Specifically, we set up a circular capturing trajectory with eight positions by evenly dividing the trajectory. We decide the height and radius of the capturing trajectory by simulating possible scenarios when the mobile user is holding the device at chest height from a reasonable distance to the reconstruction position. We choose three common human height values at $\{160, 170, 180\}$ centimeters and calculate the height of the trajectory by multiplying the user's height by 0.8 [17]. We further measure the radius of the trajectory using the number of steps and choose three possible values of $\{0.5, 1, 1.5\}$ steps and use height multiplied by 0.3 as step length [49]. For each camera observation, we export the camera HDR observation image, depth image, position, orientation, and ground truth lighting in the format of an equirectangular panorama image.

6.2.2 End-to-end Visual Quality Comparison. We compare the end-to-end rendering performance quantitatively and visually on six different virtual objects. For this experiment, we configure the simulator to run the two-field lighting reconstruction to process one near-field observation and nine far-field observations based on the guided movement policy. For near-field reconstruction, we use mesh reconstruction instead of multi-resolution projection to support the high-quality point projection. The following results showcase the visual quality upper bound LitAR can achieve.

Figure 13 shows the rendering PSNR value comparisons. Specifically, LitAR achieves 44.1% and 12.1% higher rendering PSNR than a recent deep learning-based AR lighting estimation system [66] and lighting captured by a 360° camera, on complex objects with physically-based materials (i.e., *Damaged Helmet* and *Flight Helmet*). This result indicates that by correctly leveraging user movement and scene geometry information, LitAR can generate highly accurate lighting from limited camera observations. Additionally, as we will show later in Figure 14, the rendering performance of LitAR is roughly the same with fewer observations. Note that we omit the comparison to the rendering PSNR by Xihe on metallic objects (*Metallic Sphere* and *Metallic Box*) as Xihe only provides low-frequency lighting in SH coefficients format, which does not support reflective rendering.

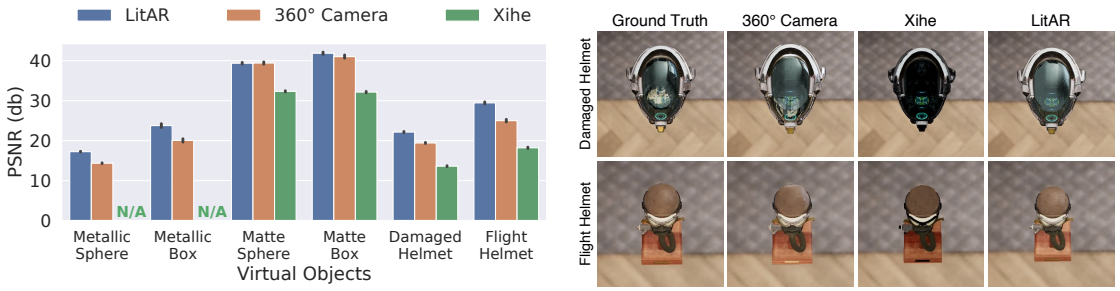

(a) PSNR comparison **(b)** Rendering visual comparison

Fig. 13. ***Simulator-based visual quality comparison.*** LitAR achieves better rendering effects, i.e., higher PSNR values (calculated against ground truth rendering), than other techniques for all objects. The PSNR comparisons to Xihe are omitted for the first four virtual objects as Xihe only provides spatial-variant low-frequency lighting estimation [66]. Virtual objects rendered with lighting provided by ground truth lighting, 360° camera, Xihe [66] and LitAR.

Figure 13b compares the visual effect of objects rendered with different lighting information. We observe that LitAR produces visually coherent virtual objects. This suggests LitAR is effective in generating a completed high-fidelity environment map. We observe that compared to ones rendered with the 360° camera observations, helmets rendered with LitAR exhibit higher structural similarity to ones rendered with ground truth lighting. For example, the two reflective regions in the lower bottom of the *Damaged Helmet* are visually separated.

6.2.3 Ablation Study of Near-field Lighting Reconstruction. This section demonstrates the effectiveness of our two-field lighting reconstruction for the near-field observation and highlights the importance of LitAR's far-field design. As we have designed LitAR to progressively improve the intermediate point cloud by naturally exploiting mobile user/device movement, we evaluate the number of near-field observations' impact on the rendering results We set up the experiment using our simulator as follows: *(i)* for each observation position, we combine camera observations from $3, 5, 7$ nearby positions on the orbiting trajectory; *(ii)* we use mesh reconstruction with LitAR for combined observations. Note that to eliminate the impact of far-field observations, we use a single dominant image color to fill the far-field portion of the environment map to simulate the ambient light sensor data. Figure 14 compares the rendering accuracy for different number of observations. We observe that the rendering PSNR values only increase *slightly* with the number of observations. This suggests that only a small portion of the environment map needs to be processed with depth information, further motivating our design choice of reconstructing near and far-field observations separately. Further, we show that rendering SSIM values increase significantly, 0.057, with the number of observations for the *Metallic Sphere* object for all ten tested reconstruction positions. This result is intuitive as more complete near-field reflections will improve the structural similarity. However, higher SSIM values do not directly translate to better PSNR values, thus implying the need to examine both metrics in quantitative studies for lighting reconstruction.

6.2.4 Ablation Study of Far-field Lighting Reconstruction. So far, we have demonstrated the effectiveness of LitAR and its spatial variance-aware near-field reconstruction component. In this section, we evaluate the performance of LitAR's directional-aware far-field lighting reconstruction and the effectiveness of our guided movement policy. We evaluate the rendering performance with a different number of guided far-field observations. Recall that guided movements naturally increase the observed scene and, therefore, allow LitAR to extrapolate environment map pixel color closer to the ground truth. Figure 15 shows the rendering performance comparison.

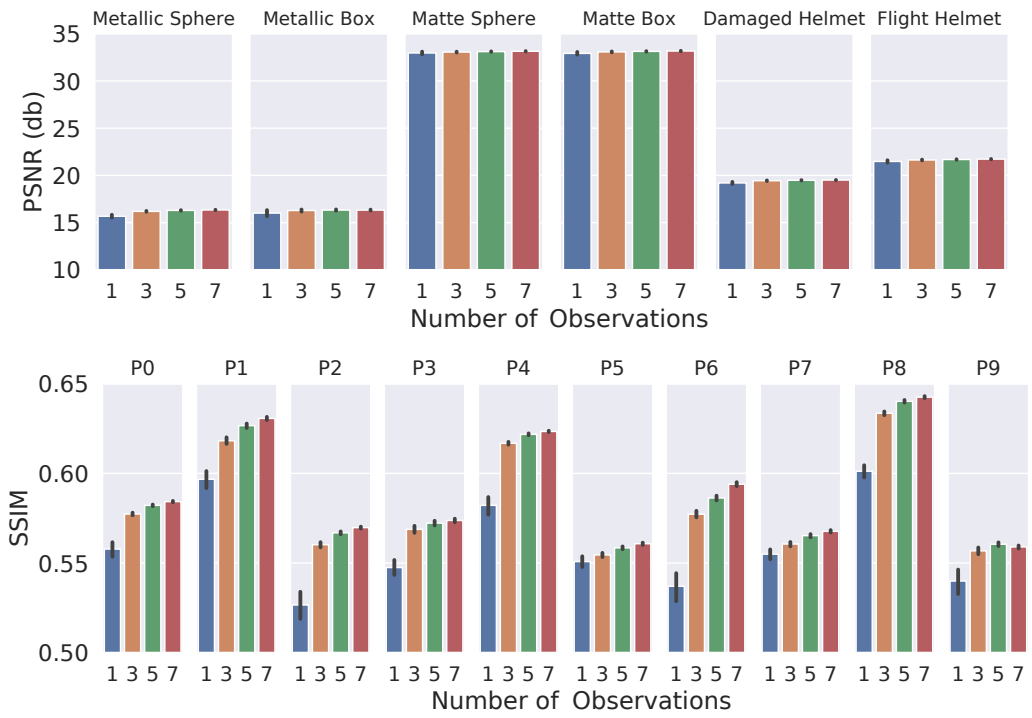

Fig. 14. ***Rendering accuracy comparison for different number of camera observations.*** The performance of LitAR, measured in PSNR, only exhibit slight improvement with more observations; while the SSIM values for more reflective materials show significant increase.

We observe that for all tested objects, having access to more guided observations improves the PSNR value by up to 31.04%. Further, we see that far-field observations exhibit different impacts on objects with different shapes. For example, both box objects see a more significant improvement than the sphere objects. This finding, if generalized, can help further improve usability by providing guided movements for different objects.

7 RELATED WORK

Mobile-specific Lighting Support. As mobile device capability increases and AR re-emerges in user-facing applications [2, 35], obtaining environment lighting for photorealistic rendering has garnered increased interests in various research communities [12, 47, 52, 65, 66]. For brevity, we only discuss works that target at lighting for indoor scenes. On the more theoretical front, Cheng et al. leveraged both the rear and front cameras to estimate spherical harmonics coefficients, low-frequency lighting representation that does not support reflection [12]. Zhao et al. proposed a two-staged pipeline called PointAR that leverages the mobile depth sensor to provide spatial-variant lighting estimation [65]. Somanath et al. introduced an efficient deep learning (DL) model called EnvMapNet that generates HDR environment map from LDR-based images [52]. In contrast to previous learning-based approaches, our work LitAR directly generates high-quality environment map with the core technique of two-field lighting reconstruction and a number of practical optimizations including multi-resolution projection. As such LitAR is not subject to common limitations of DL-based methods like training data availability and

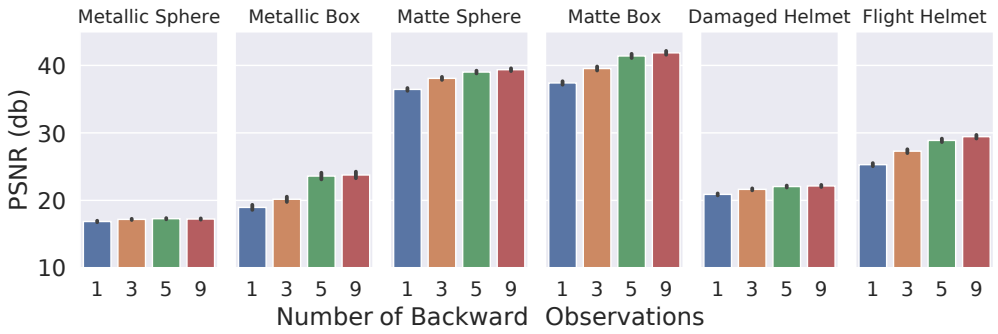

Fig. 15. ***Rendering accuracy comparison for guided movements.*** Increasing the number of backward far-field observations have different levels of improvement for tested objects.

inference performance on heterogeneous mobile resources. We also note that LitAR includes a simulator that leverages 3D indoor scenes to conduct controlled experiments, thus avoiding the need for expensive manual process of obtaining lighting ground truth.

System Supports for Lighting. On the system front, commercial SDKs such as ARKit and ARCore [25, 34] provide easy-to-use lighting estimation APIs for mobile AR application development. Two recent academic frameworks improved upon commercial offerings with GLEAM provided a real-time mobile illumination framework that supports reflective virtual objects with the use of physical probes [47], while Xihe introduced a 3D-vision based framework that provides adaptive lighting estimation [66]. We design LitAR from the outset by considering mobile characteristics including limited FoVs, natural device/user movements, and leveraging edge GPU assistance, which well positions it to reconstruct high-quality environment maps efficiently.

Image-based Lighting. In addition to mobile-specific lighting works discussed above, researchers have investigated image-based lighting [14, 15, 36], generating environment lighting representations from camera videos [28, 30, 59], and assisted lighting reconstruction with physical probes [16], object cues [55], or scene geometry [6, 41]. Recent work is mostly DL-based and can be broadly categorized as two types based on the output: estimating low-frequency lighting [24, 54] or high-frequency lighting [22, 53]. For example, Gardner et al. proposed to divide the HDR environment map learning task into two subtasks and generated one lighting estimation per image. Even though this work can handle specular object rendering, it does not consider the spatial variance. On the contrary, both Garon et al. and Lighthouse support spatial-variant lighting but are limited in rendering reflective materials [24, 54]. Our work falls in between these two types of work by generating an environment map that consists of near-field and far-field regions. This hybrid environment map allows more effective reconstruction within mobile constraints such as user movement and depth sensing accuracy while still achieving visually coherent rendering for a variety of objects including reflective ones.

8 CONCLUSION

In this work, we introduced an end-to-end lighting reconstruction system called LitAR that generates high-quality environment maps for mobile AR applications. As demonstrated both quantitatively and qualitatively, LitAR's reconstructed environment maps can be used to render objects of various properties, including reflective materials, with 14.3%/5.5% better PSNR/SSIM and visual coherence than ARKit. We showed that LitAR can produce virtual objects with more realistic and visually coherent reflection, with fine-grained visual details. For testbed-based experiments, we used physical object images to serve as the desired visual quality. Further, using

our simulator, we were able to easily compare against other techniques including Xihe and 360° camera by having access to ground truth lighting. We will open source our research artifacts to facilitate future research work in our community.

Aside from the realistic and visually coherent rendering goal, LitAR was designed with the mobile-specific constraints, e.g., limited sensing and data noise, in mind. By exploring mobile user behaviors and working within mobile sensing constraint, we proposed the two-field lighting reconstruction that divides camera observations into near-field and far-field observations based on pixels' relative distance to the reconstruction position. LitAR can work with as few as one camera observation and can progressively improve the environment map quality, especially for metallic objects, with more camera observations. Keeping usability in mind, we further introduced the motion-based automatic capture and the guided boostrapped movement policies to help AR users capture higher quality data and more suitable camera observations. LitAR significantly speeds up both the near-field and far-field reconstructions by two novel point cloud techniques multi-resolution projection and anchor extrapolation. Last but not least, LitAR provides three quality presets and exposes a number of knobs for mobile AR applications to trade-off reconstruction quality and time based on their specific use cases.

We conducted evaluations of LitAR's performance with a lab-based testbed and the game engine-based simulator. We observed that LitAR can generate higher-quality environment maps than ARKit and result in rendered objects with up to 14.3%/5.5% higher PSNR/SSIM, when compared to the physical counterpart. Further, we showed that multi-resolution projection significantly reduces the point cloud projection from 3 seconds, using mesh reconstruction, to 14.6ms. Overall, LitAR can generate about 22 high-quality environment maps per second when point cloud registration is not required. As we design the point cloud registration to run asynchronously, the registration step will not block the main reconstruction pipeline; once completed, an updated environment map will be sent to the mobile device. As part of the future work, we will explore techniques to improve the details of the generated environment maps and design runtime policies to better handle temporal variant lighting.

REFERENCES

[1] Ibraheem Alhashim and Peter Wonka. 2018. High Quality Monocular Depth Estimation via Transfer Learning. *arXiv e-prints* abs/1812.11941, Article arXiv:1812.11941 (2018). arXiv:1812.11941 https://arxiv.org/abs/1812.11941

[2] Amazon. 2020. Amazon AR View. https://www.amazon.com/adlp/arview. Accessed: 2020-7-2.

[3] Christopher Andrews, Michael K Southworth, Jennifer N A Silva, and Jonathan R Silva. 2019. Extended Reality in Medical Practice. *Curr. Treat. Options Cardiovasc. Med.* 21, 4 (March 2019), 18.

[4] Apple. 2022. ARCoachingOverlayView. https://developer.apple.com/documentation/arkit/arcoachingoverlayview.

[5] Apple. 2022. iPhone 13 Pro Tech Specs. https://www.apple.com/iphone-13-pro/specs/.

[6] Dejan Azinovic, Tzu-Mao Li, Anton Kaplanyan, and Matthias Nießner. 2019. Inverse path tracing for joint material and lighting estimation. In *Proceedings of the IEEE/CVF Conference on Computer Vision and Pattern Recognition*. IEEE, Long Beach, CA, 2447–2456.

[7] Ali J Ben Ali, Zakieh Sadat Hashemifar, and Karthik Dantu. 2020. Edge-SLAM: edge-assisted visual simultaneous localization and mapping. In *Proceedings of the 18th International Conference on Mobile Systems, Applications, and Services* (Toronto, Ontario, Canada) *(MobiSys '20)*. Association for Computing Machinery, New York, NY, USA, 325–337.

[8] F. Bernardini, J. Mittleman, H. Rushmeier, C. Silva, and G. Taubin. 1999. The ball-pivoting algorithm for surface reconstruction. *IEEE Transactions on Visualization and Computer Graphics* 5, 4 (1999), 349–359. https://doi.org/10.1109/2945.817351

[9] Paul J Besl and Neil D McKay. 1992. Method for registration of 3-D shapes. In *Sensor fusion IV: control paradigms and data structures*, Vol. 1611. Spie, 586–606.

[10] Dan Cernea. 2020. OpenMVS: Multi-View Stereo Reconstruction Library. (2020). https://cdcseacave.github.io/openMVS

[11] Angel Chang, Angela Dai, Thomas Funkhouser, Maciej Halber, Matthias Niebner, Manolis Savva, Shuran Song, Andy Zeng, and Yinda Zhang. 2017. Matterport3D: Learning from RGB-D Data in Indoor Environments. In *2017 International Conference on 3D Vision (3DV)*. IEEE Computer Society, 667–676.

[12] Dachuan Cheng, Jian Shi, Yanyun Chen, Xiaoming Deng, and Xiaopeng Zhang. 2018. Learning Scene Illumination by Pairwise Photos from Rear and Front Mobile Cameras. *Comput. Graph. Forum* 37, 7 (2018), 213–221. http://dblp.uni-trier.de/db/journals/cgf/cgf37.html#ChengSCDZ18

[13] RidgeRun Embedded Linux Developer Connection. 2022. NVIDIA CUDA Memory Management. https://developer.ridgerun.com/wiki/index.php?title=NVIDIA_CUDA_Memory_Management.

[14] Massimiliano Corsini, Marco Callieri, and Paolo Cignoni. 2008. Stereo light probe. In *Computer Graphics Forum*, Vol. 27. Wiley Online Library, 291–300.

[15] Paul Debevec. 2006. Image-based lighting. In *ACM SIGGRAPH 2006 Courses*. 4–es.

[16] Paul Debevec. 2008. Rendering synthetic objects into real scenes: Bridging traditional and image-based graphics with global illumination and high dynamic range photography. In *ACM SIGGRAPH 2008 classes*. 1–10.

[17] Devin Larson. 2014. Standard Proportions of the Human Body. https://www.makingcomics.com/2014/01/19/standard-proportions-human-body/. Accessed: 2021-11-5.

[18] Ufuk Dilek and Mustafa Erol. 2018. Detecting position using ARKit II: generating position-time graphs in real-time and further information on limitations of ARKit. *Physics Education* 53, 3 (2018), 035020.

[19] Ruofei Du, Eric Turner, Maksym Dzitsiuk, Luca Prasso, Ivo Duarte, Jason Dourgarian, Joao Afonso, Jose Pascoal, Josh Gladstone, Nuno Cruces, Shahram Izadi, Adarsh Kowdle, Konstantine Tsotsos, and David Kim. 2020. DepthLab: Real-Time 3D Interaction With Depth Maps for Mobile Augmented Reality. In *Proceedings of the 33rd Annual ACM Symposium on User Interface Software and Technology (UIST)*. ACM, 15 pages. https://doi.org/10.1145/3379337.3415881

[20] Farshad Einabadi, Jean-Yves Guillemaut, and Adrian Hilton. 2021. Deep neural models for illumination estimation and relighting: A survey. *Comput. Graph. Forum* 40, 6 (Sept. 2021), 315–331.

[21] Epic Games. 2021. Unreal Engine - Real-Time 3D Creation Tool. https://www.unrealengine.com. Accessed: 2021-11-5.

[22] Marc-André Gardner, Kalyan Sunkavalli, Ersin Yumer, Xiaohui Shen, Emiliano Gambaretto, Christian Gagné, and Jean-François Lalonde. 2017. Learning to Predict Indoor Illumination from a Single Image. *ACM Transactions on Graphics* (2017).

[23] Marc-Andre Gardner, Yannick Hold-Geoffroy, Kalyan Sunkavalli, Christian Gagne, and Jean-Francois Lalonde. 2019. Deep Parametric Indoor Lighting Estimation.

[24] Mathieu Garon, Kalyan Sunkavalli, Sunil Hadap, Nathan Carr, and Jean-François Lalonde. 2019. Fast Spatially-Varying Indoor Lighting Estimation. *CVPR* (2019).

[25] Google. 2020. ARCore. https://developers.google.com/ar.

[26] Google. 2022. Pixel 6 Tech Specs. https://store.google.com/product/pixel_6_specs?hl=en-US.

[27] Google for Education. 2022. Bringing virtual and augmented reality to school | Google for Education. https://edu.google.com/products/vr-ar/?modal_active=none. Accessed: 2020-7-24.

[28] Thorsten Grosch, Tobias Eble, and Stefan Mueller. 2007. Consistent interactive augmentation of live camera images with correct near-field illumination. In *Proceedings of the 2007 ACM symposium on Virtual reality software and technology*. 125–132.

[29] Charles R. Harris, K. Jarrod Millman, Stéfan J. van der Walt, Ralf Gommers, Pauli Virtanen, David Cournapeau, Eric Wieser, Julian Taylor, Sebastian Berg, Nathaniel J. Smith, Robert Kern, Matti Picus, Stephan Hoyer, Marten H. van Kerkwijk, Matthew Brett, Allan Haldane, Jaime Fernández del Río, Mark Wiebe, Pearu Peterson, Pierre Gérard-Marchant, Kevin Sheppard, Tyler Reddy, Warren Weckesser, Hameer Abbasi, Christoph Gohlke, and Travis E. Oliphant. 2020. Array programming with NumPy. *Nature* 585, 7825 (Sept. 2020), 357–362. https://doi.org/10.1038/s41586-020-2649-2

[30] Vlastimil Havran, Miloslaw Smyk, Grzegorz Krawczyk, Karol Myszkowski, and Hans-Peter Seidel. 2005. Interactive System for Dynamic Scene Lighting using Captured Video Environment Maps.. In *Rendering Techniques*. 31–42.

[31] HUAWEI. 2021. HUAWEI Mate 30 Pro Specifications | HUAWEI Global. https://consumer.huawei.com/en/phones/mate30-pro/specs/. Accessed: 2020-7-8.

[32] Apple Inc. 2020. iPad Pro 2020. https://www.apple.com/ipad-pro/specs/.

[33] Apple Inc. 2022. Adding Realistic Reflections to an AR Experience. https://developer.apple.com/documentation/arkit/camera_lighting_and_effects/adding_realistic_reflections_to_an_ar_experience.

[34] Apple Inc. 2022. Introducing ARKit 5. https://developer.apple.com/augmented-reality/arkit/.

[35] Inter IKEA Systems B. V. 2017. IKEA Place. https://apps.apple.com/us/app/ikea-place/id1279244498. Accessed: 2020-7-2.

[36] Brian Karis and Epic Games. 2013. Real shading in unreal engine 4. *Proc. Physically Based Shading Theory Practice* 4, 3 (2013).

[37] Siu Kwan Lam, Antoine Pitrou, and Stanley Seibert. 2015. Numba: A LLVM-Based Python JIT Compiler. In *Proceedings of the Second Workshop on the LLVM Compiler Infrastructure in HPC* (Austin, Texas) *(LLVM '15)*. Association for Computing Machinery, New York, NY, USA, Article 7, 6 pages. https://doi.org/10.1145/2833157.2833162

[38] Junxuan Li, Hongdong Li, and Yasuyuki Matsushita. 2021. Lighting, Reflectance and Geometry Estimation From 360deg Panoramic Stereo. In *Proceedings of the IEEE/CVF Conference on Computer Vision and Pattern Recognition (CVPR)*. 10591–10600.

[39] Zhengqin Li, Mohammad Shafiei, Ravi Ramamoorthi, Kalyan Sunkavalli, and Manmohan Chandraker. 2020. Inverse rendering for complex indoor scenes: Shape, spatially-varying lighting and svbrdf from a single image. In *Proceedings of the IEEE/CVF Conference on Computer Vision and Pattern Recognition*. 2475–2484.

[40] Z Liu, G Lan, J Stojkovic, Y Zhang, C Joe-Wong, and M Gorlatova. 2020. CollabAR: Edge-assisted Collaborative Image Recognition for Mobile Augmented Reality. In *2020 19th ACM/IEEE International Conference on Information Processing in Sensor Networks (IPSN)*. 301–312.

[41] Robert Maier, Kihwan Kim, Daniel Cremers, Jan Kautz, and Matthias Nießner. 2017. Intrinsic3D: High-Quality 3D Reconstruction by Joint Appearance and Geometry Optimization with Spatially-Varying Lighting. (Aug. 2017). arXiv:1708.01670 [cs.CV]

[42] Morgan McGuire and Michael Mara. 2014. Efficient GPU screen-space ray tracing. *Journal of Computer Graphics Techniques (JCGT)* 3, 4 (2014), 73–85.

[43] Pierre Moulon, Pascal Monasse, Romuald Perrot, and Renaud Marlet. 2016. OpenMVG: Open multiple view geometry. In *International Workshop on Reproducible Research in Pattern Recognition*. Springer, 60–74.

[44] Raúl Mur-Artal and Juan D. Tardós. 2017. ORB-SLAM2: an Open-Source SLAM System for Monocular, Stereo and RGB-D Cameras. *IEEE Transactions on Robotics* 33, 5 (2017), 1255–1262. https://doi.org/10.1109/TRO.2017.2705103

[45] Nvidia. 2022. Jetson AGX Xavier Developer Kit. https://developer.nvidia.com/embedded/jetson-agx-xavier-developer-kit.

[46] Rohit Pandey, Sergio Orts Escolano, Chloe Legendre, Christian Häne, Sofien Bouaziz, Christoph Rhemann, Paul Debevec, and Sean Fanello. 2021. Total relighting: learning to relight portraits for background replacement. *ACM Trans. Graph.* 40, 4 (July 2021), 1–21.

[47] Siddhant Prakash, Alireza Bahremand, Linda D Nguyen, and Robert LiKamWa. 2019. Gleam: An illumination estimation framework for real-time photorealistic augmented reality on mobile devices. In *Proceedings of the 17th Annual International Conference on Mobile Systems, Applications, and Services*. 142–154.

[48] René Ranftl, Katrin Lasinger, David Hafner, Konrad Schindler, and Vladlen Koltun. 2020. Towards Robust Monocular Depth Estimation: Mixing Datasets for Zero-shot Cross-dataset Transfer. *IEEE Transactions on Pattern Analysis and Machine Intelligence (TPAMI)* (2020).

[49] Science Buddies. 2013. Stepping Science: Estimating Someone's Height from Their Walk. https://www.scientificamerican.com/article/bring-science-home-estimating-height-walk/. Accessed: 2021-11-5.

[50] Sciontidesign. 2021. Archviz Interior Rendering. https://docs.unrealengine.com/4.27/en-US/Resources/Showcases/ArchVisInterior/. Accessed: 2021-11-5.

[51] Scott Stein. 2021. Lidar is one of the iPhone and iPad's coolest tricks. Here's what else it can do. https://www.cnet.com/tech/mobile/lidar-is-one-of-the-iphone-ipad-coolest-tricks-its-only-getting-better/. Accessed: 2021-11-5.

[52] Gowri Somanath and Daniel Kurz. 2021. HDR Environment Map Estimation for Real-Time Augmented Reality. *CVPR* (2021).

[53] Shuran Song and Thomas Funkhouser. 2019. Neural Illumination: Lighting Prediction for Indoor Environments. *CVPR* (2019).

[54] Pratul P. Srinivasan, Ben Mildenhall, Matthew Tancik, Jonathan T. Barron, Richard Tucker, and Noah Snavely. 2020. Lighthouse: Predicting Lighting Volumes for Spatially-Coherent Illumination. In *CVPR*.

[55] Tiancheng Sun, Jonathan T Barron, Yun-Ta Tsai, Zexiang Xu, Xueming Yu, Graham Fyffe, Christoph Rhemann, Jay Busch, Paul Debevec, and Ravi Ramamoorthi. 2019. Single image portrait relighting. *ACM Trans. Graph.* 38, 4 (July 2019), 1–12.

[56] Three.js Organization. 2021. Three.js - JavaScript 3D library. https://threejs.org. Accessed: 2021-11-5.

[57] TornadoWeb. 2022. Tornado Web Server. https://www.tornadoweb.org/en/stable/.

[58] Mihran Tuceryan et al. 2019. AR360: dynamic illumination for augmented reality with real-time interaction. In *2019 IEEE 2nd International Conference on Information and Computer Technologies (ICICT)*. IEEE, 170–174.

[59] Jonas Unger, Joel Kronander, Per Larsson, Stefan Gustavson, and Anders Ynnerman. 2013. Temporally and spatially varying image based lighting using HDR-video. In *21st European Signal Processing Conference (EUSIPCO 2013)*. IEEE, Marrakech, Morocco, 1–5.

[60] Unity. 2020. AR Foundation 4.2.0-preview.5. https://docs.unity3d.com/Packages/com.unity.xr.arfoundation@4.2/manual/index.html.

[61] Unity3D. 2022. Unity3D. https://docs.unity3d.com/. Accessed: 2022-5-14.

[62] Jingao Xu, Guoxuan Chi, Zheng Yang, Danyang Li, Qian Zhang, Qiang Ma, and Xin Miao. 2021. FollowUpAR: enabling follow-up effects in mobile AR applications. In *Proceedings of the 19th Annual International Conference on Mobile Systems, Applications, and Services* (Virtual Event, Wisconsin) *(MobiSys '21)*. Association for Computing Machinery, New York, NY, USA, 1–13.

[63] Juheon Yi and Youngki Lee. 2020. Heimdall: mobile GPU coordination platform for augmented reality applications. In *Proceedings of the 26th Annual International Conference on Mobile Computing and Networking* (London, United Kingdom) *(MobiCom '20, Article 35)*. Association for Computing Machinery, New York, NY, USA, 1–14.

[64] Yunfan Zhang, Tim Scargill, Ashutosh Vaishnav, Gopika Premsankar, Mario Di Francesco, and Maria Gorlatova. 2022. InDepth: Real-Time Depth Inpainting for Mobile Augmented Reality. *Proc. ACM Interact. Mob. Wearable Ubiquitous Technol.* 6, 1, Article 37 (mar 2022), 25 pages. https://doi.org/10.1145/3517260

[65] Yiqin Zhao and Tian Guo. 2020. PointAR: Efficient Lighting Estimation for Mobile Augmented Reality. In *Computer Vision – ECCV 2020*, Andrea Vedaldi, Horst Bischof, Thomas Brox, and Jan-Michael Frahm (Eds.). Springer International Publishing, Cham, 678–693.

[66] Yiqin Zhao and Tian Guo. 2021. Xihe: A 3D Vision-Based Lighting Estimation Framework for Mobile Augmented Reality. In *Proceedings of the 19th Annual International Conference on Mobile Systems, Applications, and Services* (Virtual Event, Wisconsin) *(MobiSys '21)*. Association for Computing Machinery, New York, NY, USA, 28–40. https://doi.org/10.1145/3458864.3467886